1986

Contribution to Power System Harmonic Analysis.

Yahia Baghzouz
Louisiana State University and Agricultural & Mechanical College

Baghzouz, Yahia

CONTRIBUTION TO POWER SYSTEM HARMONIC ANALYSIS

The Louisiana State University and Agricultural and Mechanical Col. PH.D. 1986

PLEASE NOTE:

In all cases this material has been filmed in the best possible way from the available copy. Problems encountered with this document have been identified here with a check mark __✓__.

1. Glossy photographs or pages _____
2. Colored illustrations, paper or print _____
3. Photographs with dark background _____
4. Illustrations are poor copy _____
5. Pages with black marks, not original copy _____
6. Print shows through as there is text on both sides of page _____
7. Indistinct, broken or small print on several pages ✓
8. Print exceeds margin requirements _____
9. Tightly bound copy with print lost in spine _____
10. Computer printout pages with indistinct print _____
11. Page(s) _____ lacking when material received, and not available from school or author.
12. Page(s) _____ seem to be missing in numbering only as text follows.
13. Two pages numbered _____. Text follows.
14. Curling and wrinkled pages _____
15. Dissertation contains pages with print at a slant, filmed as received _____
16. Other _____

University
Microfilms
International

CONTRIBUTION TO POWER SYSTEM HARMONIC ANALYSIS

A Dissertation

Submitted to the Graduate Faculty of the
Louisiana State University and
Agricultural and Mechanical College
in partial fulfillment of the
requirements for the degree of
Doctor of Philosophy

in

The Department of Electrical and Computer Engineering

by
Yahia Baghzouz
B.S., Louisiana State University, May,1981
M.S., Louisiana State University, December, 1982
May 1986

ACKNOWLEDGMENTS

The author wishes to express his gratitude and appreciation to Dr. Owen T. Tan for his unique friendship and guidance throughout the author's graduate program and his valuable assistance in the preparation of this dissertation. Appreciation is also expressed to Dr. Gill G. Richards, Dr. Ali Mirbod and Dr. William A. Porter of the Electrical and Computer Engineering Department, and Dr. James R. Dorroh of the Department of Mathematics for serving as members of the examining committee.

The financial assistance of the Electrical and Computer Engineering Department and the Electric Power Research Consortium, sponsored by Louisiana Power and Light Co., Gulf States Utilities Co. and Southwestern Power Co., is greatly acknowledged.

The author would like to express his deepest appreciation to his parents, his brothers and sisters for their love and support throughout his undergraduate and graduate studies. Finally, the author's sincere appreciation goes to his wife Chanpheng for her patience and constant encouragement.

TABLE OF CONTENTS

ACKNOWLEDGMENTS. ii

TABLE OF CONTENTS. iii

LIST OF TABLES vi

LIST OF FIGURES. vii

ABSTRACT viii

1. INTRODUCTION. 1

2. OVERVIEW ON POWER SYSTEM HARMONICS. 6

2.1 Harmonic Sources. 6

2.1.1 Static Power Converters 6

2.1.2 Other Harmonic Sources. 10

2.2 Harmonic Effects. 12

2.2.1 Power Components 12

2.2.2 Electric Instruments 14

2.2.3 Power Factor 16

2.2.4 Communication Systems. 17

2.3 Methods of Reducing Harmonic Levels 17

2.3.1 Harmonic Cancellation. 18

2.3.2 Harmonic Filtering 19

2.3.3 Alternative Methods. 21

3. METHODS OF PREDICTING HARMONIC LEVELS 23

3.1 System Component Models 24

3.2 Harmonic Analysis Methods 29

3.2.1 Nonlinear Time Domain Analysis 29

3.2.2 Nonlinear Frequency Domain Analysis. 30

3.2.3 Linear Frequency Domain Analysis 32

4. PROBABILISTIC MODELING OF POWER SYSTEM HARMONICS. 36

4.1 Classification of Nonlinear Loads 38

4.2 Probability Distribution of Harmonic Injection. 39

4.2.1 Sum of Random Number of Constant Currents. 42

4.2.2 Sum of Constant Number of Random Currents. 42

4.2.3 Sum of Random Number of Random Currents. 44

4.2.4 Resultant n-th Harmonic Current Injection. 45

4.3 Probability Distribution of Harmonic Propagation. 46

4.4 Computational Methods 48

4.5 Example and Discussion of Results 49

4.5.1 Statistical Data of Nonlinear Loads. 51

4.5.2 Simulation Results and Discussion. 54

4.6 Potential Applications. 58

4.6.1 Setting Limitations on Harmonic Levels 58

4.6.2 Power Factor Correction. 59

4.6.3 Communication Interference 60

4.6.4 Estimating Line Losses 60

4.6.5 Equipment Design 61

5. MAXIMUM HEATING AND INSULATION STRESS ON UNTRANSPOSED TRANSMISSION LINES UNDER NONSINUSOIDAL CONDITIONS. 62

5.1 Expression for Single Harmonic. 63

5.2 Maximum Single Harmonic Current and Voltage 66

5.2.1 Global Convergence Method 67

5.2.2 Local Convergence Method. 69

5.3 Maximum Overall RMS Current and Peak Voltage. 71

5.4 Maximum Distortion Factor 78

5.5 Single-Phase Lines. 78

5.6 Numerical Example and Discussion of Results 80

6. CONCLUSIONS 88

REFERENCES 90

APPENDIX I: HARMONIC COMPUTATION OF DISTORTED WAVEFORMS 96

APPENDIX II: EQUIVALENT SERIES IMPEDANCE AND SHUNT ADMITTANCE OF TRANSMISSION LINES. 98

VITA 102

LIST OF TABLES

TABLE I. System Component Models. 25

TABLE II. Harmonic Levels (% of Fundamental) and their Phase Angles (Degrees w.r.t. V_a^1) at Receiving Line End. 82

TABLE III. Computed Global Maxima and Locations of RMS Currents, Peak Voltages and Distortion Factors 83

LIST OF FIGURES

Fig. 1. Converter Equivalent Circuit: (a) Rectifier, (b) Inverter. . 7

Fig. 2. Twelve-Pulse Converter Configuration 18

Fig. 3. Reduced Equivalent Circuit of Converter-Filter-Power Network 20

Fig. 4. Induction Motor Model: (a) Exact, (b) Approximate. 27

Fig. 5. Simplest Equivalent Circuit for Harmonic Analysis. 33

Fig. 6. Power System with Multiple Nonlinear Loads 34

Fig. 7. Load Composition 41

Fig. 8. Flowchart of Integration Method. 50

Fig. 9. Flowchart of Monte Carlo Simulation Method 51

Fig. 10. Three-Bus Distribution System: (a) One-Line Diagram, (b) Equivalent Circuit for 5-th Harmonic 52

Fig. 11. 5-th Harmonic Current Generated by Typical Battery Charger . 53

Fig. 12. PDFs of (a) Real and (b) Imaginary Parts of 5-th Harmonic Current in Time Intervals 2, 3 and 4 55

Fig. 13. PDFs of Random Component of 5-th Harmonic Current Magnitude in Time Intervals 2, 3 and 4 56

Fig. 14. Expected Value of 5-th Harmonic Current Versus Time. 57

Fig. 15. PDFs of Random Component of 5-th Harmonic Voltage Magnitude at Bus 3 in Time Intervals 2, 3 and 4. 57

Fig. 16. Flowchart of Global Convergence Method 69

Fig. 17. Flowchart of Local Convergence Method. 72

Fig. 18. Flowchart for Computing Maximum Peak Voltage 77

Fig. 19. Three-Phase Transmission Line (Phase Wires: 795000 CM 26/7 ACSR; Steel Ground Wires: R = 4 Ω/mi, and GMR = 0.001 ft). . 81

Fig. 20. Variation of RMS Currents. 84

Fig. 21. Variation of Peak (a) Phase Voltages and (b) Line Voltages . 85

Fig. 22. Distortion Factor of (a) Currents, (b) Phase Voltages and (c) Line Voltages. 86

Fig. 23. Instantaneous Phase 'a' Voltage in Search Region 87

ABSTRACT

In recent years, power system harmonic levels have increased significantly due to the ever-increasing use of nonlinear loads which primarily consist of power electronic devices. The effect of these harmonics on power system components represents a serious problem to utility companies and consumers.

A survey of power system harmonics as generated mainly by static ac/dc power converters is presented. Aspects concerning harmonic injection, their effects on system components and harmonic reduction techniques are included. Harmonic analysis methodologies are discussed and compared in terms of efficiency and accuracy.

The need of a stochastic treatment of harmonic voltages and currents is clearly explained. A novel probabilistic model of analyzing power system harmonics is developed. Depending on their operating modes and switching states, nonlinear loads connected to each distribution bus are decomposed into four distinct categories of harmonic current injection. The probability distribution of the total random current injected at each bus is determined after making some reasonable assumptions. Probability characteristics of the resulting harmonic voltages are calculated. Two computational methods, i.e., the direct integration method and the Monte Carlo simulation method, are presented for determining the statistical characteristics of the harmonic signals. The procedure is demonstrated by an example which illustrates the probability aspects of power system harmonics. Potential applications of the probabilistic model are also considered.

In harmonic modeling of a transmission line, the use of the π-equivalent does not provide the location of maximum heating and insulation stress on the line. In this study, the differential equations describing voltage and current wave propagation along transmission lines are solved by modal decomposition. The resulting solution is transformed back into phase quantities. Two efficient numerical algorithms are developed to compute and locate maximum heating and insulation stress on untransposed transmission lines with distorted voltage and current waveforms. The numerical algorithms developed will guarantee convergence to the global solution. Other applications of these algorithms, such as determining maximum values of individual harmonics for communication interference studies and maximum distortion factors on the transmission lines, are included. The numerical methods are demonstrated by an example.

1. INTRODUCTION

The existence of voltage and current distortion on power systems has been recognized since the early days of alternating current. In the past, harmonic sources were limited to transformers caused by saturation and electric machines. In most cases, harmonic magnitudes were very limited and could be reduced to acceptable levels through the use of wye-delta transformer connections [1].

In the last two decades, however, the number of nonlinear loads has rapidly increased due to the recent advances in high power semiconductor switching devices. The prolification of power converters which are widely used in high voltage direct current (HVDC) transmission, motor speed control, uninterrupted power supplies (UPS), battery chargers and photovoltaic stations suggests a renewed look at harmonic signals in power systems [2]. Furthermore, in the near future, electric utilities anticipate installing energy storage devices and their associated ac/dc converter equipment on distribution feeders to augment central-station power supplies [3]; hence, harmonic sources will continue to increase.

Today, it is clear that power system harmonics are becoming a very serious problem which represents for the first time a potential of disturbing the normal operation of both consumer loads and power network. The effect of harmonics on power apparatus [4]-[5], instruments [6]-[7] and communication systems [8]-[9] represents serious problems to utility companies. Therefore, harmonic consideration for any industrial power system commands as much attention as short circuit and overvoltage considerations [2].

Harmonic problems can be investigated by actually measuring the

harmonics or by digital computer simulation. But considering the high cost and complexity of field measurements at different locations [10]-[11], utility companies have a deep interest in predicting harmonic levels analytically.

Recently, methods calculating the generation and propagation of harmonic currents in power systems under steady-state conditions have been developed [12]-[14]. In these studies, harmonic analysis is usually performed with truncated Fourier series representation of the non-sinusoidal voltages and currents, and power system elements have been represented by passive impedances which are adjusted for each harmonic frequency.

These power system harmonic programs have been inherently deterministic in nature. Any random changes in the harmonic current injection are, therefore, not reflected in the harmonic current flows and resulting harmonic voltages. In practice, it is has been recognized [15] that power system harmonics, particularly at the residential and commercial levels, are time-variant due to stochastic changes in the operating modes of nonlinear loads. Consequently, probabilistic models of harmonic injection and propagation are highly desirable for a more realistic prediction of harmonic levels [16].

Few publications dealt with the probability characteristics of harmonic current injection generated by a specific number of identical nonlinear loads including battery chargers [17], TV receivers and light dimmers [18], and d.c. motor drives [19]. But in general, nonlinear loads of different categories may be connected to a common distribution bus, and may have operating modes which are partly deterministic and partly random. In addition, the configuration or switching state of

nonlinear loads may be fixed, varying deterministically or randomly with time.

The harmonic levels in high voltage power systems, especially those generated by HVDC stations, are found to be practically constant in nature [11]. Consequently, harmonic currents and voltages can be predicted by conventional power system harmonic programs [12]-[14] where transmission lines are represented by their π-equivalent circuit. Since the long line π-equivalent circuit is a two-port network, only the terminal voltages and currents of the transmission line can be calculated. As a result, possible maximum values of the overall rms current and peak voltage along the line due to standing wave phenomena are not readily known. These maxima could be larger than the corresponding values at the line terminals and if ignored, insulation damage, overheating or communication interference could take place.

Shultz et al. [20] presented a method to compute the maximum value of a single harmonic current or voltage on an equivalent single-phase transmission line. However, it is recognized that the maximum overall rms current and total peak voltage are of greater importance. Furthermore, transmission lines are generally multiphase and often untransposed [21], thus cannot be represented by an equivalent single-phase line.

The objective of this study is (1) to develop a probabilistic method of modeling power system harmonics, and (2) to develop efficient numerical methods for locating and computing the maximum line heating and insulation stress on unbalanced transmission lines under nonsinusoidal conditions. Before these specific problems are considered, an overview on power system harmonics and discussion of the existing harmonic study

methodologies are given. The material is arranged in four chapters.

Chapter 2 gives an overview of power system harmonics including harmonic sources, their effects on power system components and existing methods of harmonic compensation. The major source of harmonics is the static power converter. Other sources of harmonics include transformer saturation, electric machines, arc furnaces and welders, gaseous discharge lighting and static VAR compensators. Power system harmonics are known to affect most power system apparatus, power instruments and communication systems. The most popular harmonic mitigation techniques consist of harmonic cancellation and harmonic filtering methods. Alternative methods of harmonic compensation, such as current injection and magnetic flux compensation, have not been developed for high power ratings.

Chapter 3 discusses power system component models and methods of harmonic analysis; namely, the piece-wise linear time-domain analysis, the nonlinear frequency-domain analysis and the linear frequency-domain analysis. The methods are compared in terms of their accuracy and complexity. The most efficient and widely used method is the linear frequency-domain simulation method, but the most accurate tool yet developed is the nonlinear frequency-domain method.

Chapter 4 introduces a probabilistic modeling of power system harmonics and provides two numerical algorithms for computing the probability characteristics of harmonic currents and voltages. After classifying nonlinear loads into four different categories in terms of their operating modes, probability distributions of harmonic current injection and propagation are derived. The probabilistic method of harmonic analysis is demonstrated by an example, and potential applica-

tions of this method are discussed.

Finally, the problem of locating and computing maximum heating (maximum total rms current) and insulation stress (maximum overall peak voltage) on unbalanced transmission lines under nonsinusoidal conditions is investigated in chapter 5. Two numerical methods for computing the maximum rms current and an algorithm to find the maximum peak voltage, both of which guarantee convergence to the global solution, are developed. Other applications of the algorithms, such as computing the maximum of each current harmonic for finding the telephone influence factor and maximum distortion factors for conforming with harmonic limits, are included. The special cases of single-phase and balanced three-phase transmission lines are considered. The numerical methods are illustrated by an example.

2. OVERVIEW ON POWER SYSTEM HARMONICS

A brief review on sources of power systems harmonics, harmonic effects on power equipment and instrumentation and various methods of harmonic compensation is given in this chapter. Most of the material is taken from Ref. [22] which provides a concise survey of harmonic generation, analysis, interference and reduction. A more rigorous and exhaustive treatment of these subjects can be found in several publications, particularly those by Kimbark [23], Arrillaga et al. [4] and the IEEE tutorial course on power system harmonics [5]. Reference [24] also gives a fairly complete bibliography of studies on power system harmonics.

2.1 Harmonic Sources

Power system voltage and current harmonics result from the nonlinear operating characteristics of certain power sytem components. Existing analytical [25] and numerical [26] methods for computing the harmonic levels of nonsinusoidal waveforms are summarized in Appendix I. The most common power apparatus known to generate harmonics are discussed in this section. Emphasis is given to static power converters since they are widely used for a wide range of power ratings and represent the major source of harmonics.

2.1.1 Static Power Converters

It has been recognized that phase-controlled rectifiers and inverters represent the main harmonic source in power and distribution systems [2]. These converters are conveniently grouped in terms of their power ratings: high, medium and low power converters. Each of

these groups will be briefly discussed.

Large power rectifiers, such as those used in high voltage d.c. transmission (HVDC), generally have a large inductance on the d.c. side. The direct current is thus reasonably constant and the rectifier acts like a harmonic current source on the a.c. side as shown by the equivalent circuit in Fig. 1(a). For the ideal case of instantaneous commutation between the conducting elements, a p-pulse converter generates characteristic current harmonics of the order

$$n = pk \pm 1, \quad k = 1,2,3... \tag{1}$$

with their rms value given by [23]

$$I_n = I_1/n = \sqrt{6}\, I_d/n\pi$$

where I_1 is the fundamental current (with no overlap) and I_d is the converter direct current.

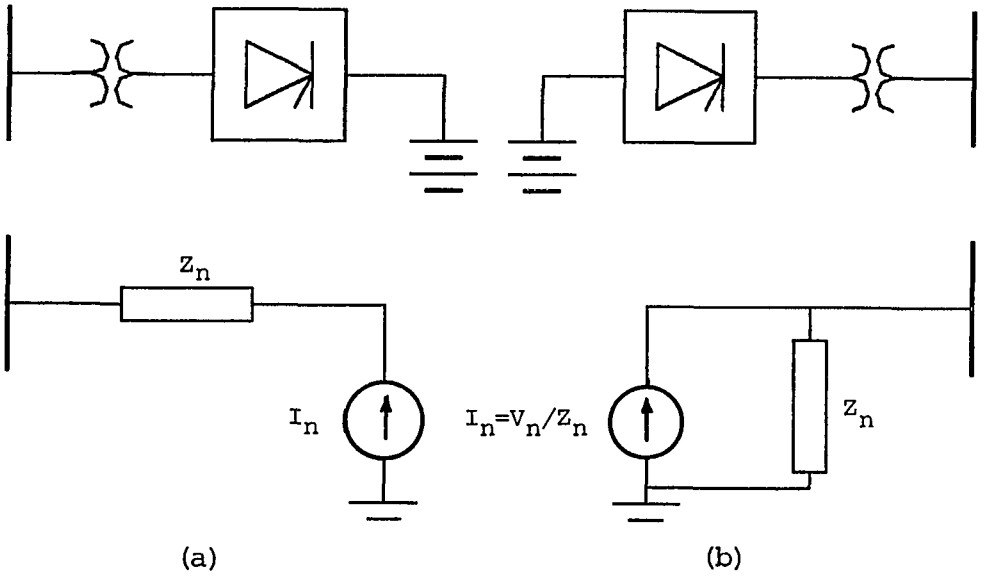

Fig. 1. Converter Equivalent Circuit: (a) Rectifier, (b) Inverter.

If a Y-Y connected transformer is used at the terminals of a 6-pulse rectifier, then the frequency domain representation of line current is

$$i(t) = \frac{2\sqrt{3}}{\pi} I_d \{\cos(\omega t) - \frac{1}{5}\cos(5\omega t) + \frac{1}{7}\cos(7\omega t) - \frac{1}{11}\cos(11\omega t) + \frac{1}{13}\cos(13\omega t) \ldots\}. \quad (2)$$

On the other hand, when either the primary or secondary windings of the rectifier transformer are connected in delta, the line current in (2) becomes

$$i(t) = \frac{2\sqrt{3}}{\pi} I_d \{\cos(\omega t) + \frac{1}{5}\cos(5\omega t) - \frac{1}{7}\cos(7\omega t) + \frac{1}{11}\cos(11\omega t) - \frac{1}{13}\cos(13\omega t) \ldots\}. \quad (3)$$

If the commutation period is taken into account, the magnitude of the n-th current harmonic is given by [23]

$$I_n = I_1 \, F(\alpha,\beta)/2Dn = \sqrt{3} \, V \, F(\alpha,\beta)/2\pi\omega nL \quad (4)$$

where

$$D = \cos(\alpha) - \cos(\alpha+\beta)$$

$$F(\alpha,\beta) = 2[(S_1)^2 + (S_2)^2 - 2S_1S_2\cos(\alpha+\beta)]^{\frac{1}{2}}$$

with

$$S_1 = \frac{\sin\{(n+1)\beta/2\}}{(n+1)}$$

and

$$S_2 = \frac{\sin\{(n-1)\beta/2\}}{(n-1)}.$$

Herein, ωL is the equivalent short-circuit reactance, α is the firing angle and β is the commutation angle.

In addition to the characteristic current harmonics, harmonics of uncharacteristic orders are also produced. These harmonics are caused by unbalanced voltages and line impedances or by unequal thyristor firing angles. The uncharacteristic harmonics are normally much smaller

than the corresponding adjacent characteristic harmonics. It is suggested that uncharacteristic harmonics of order (6n-1) and (6n+1), n=1,3,... for a 12-pulse converter be approximated to 15% of the level computed for a 6-pulse converter [27], whereas noncharacteristic odd multiples of the third harmonic , i.e., 3n, n=1,3,..., be set to 1% of the fundamental [28].

Large power inverters, found at the receiving end of an HVDC transmission line, are represented by characteristic harmonic voltage sources behind a series impedance. The voltage magnitude for each characteristic frequency depends on the control technique used to regulate the fundamental voltage. The values of the voltage harmonic magnitudes, their phase angles and series impedances can be obtained from the manufacturer. It is noted that for analysis purposes, the harmonic voltage source can be converted into an equivalent harmonic current source by Norton's theorem as shown in Fig. 1(b).

Medium power converters are gaining wide application in motor speed control due to recent advances in power switching devices. Direct current drives, which still hold a big share of motor drives, generate harmonic currents which depend on the relatively small inductance on the d.c. side of the converter [29]. On the other hand, the current harmonics generated by a.c. drives depend on the motor speed and the type of control arrangement used. The most common types of control for such drives include a.c. voltage control, variable-voltage variable-frequency control, variable-current variable-frequency control, and pulse-width-modulation control. The harmonic currents injected by each of these drives are well documented in Ref. [30].

Low Power Converters are used in several home appliances (TV and stereo receivers, microwaves, desk computers) and office systems (computers). Other devices employing power electronic switches include light dimmers, heating control units and battery chargers. Because of their low power ratings, these converters inject relatively small harmonic currents into the utility supply, but if the use of electric vehicles becomes widely accepted, battery chargers will become a major source of harmonics [31].

2.1.2 Other Harmonic Sources

Before the development of static power converters, harmonic distortion was primarily associated with electric machines and transformers. Other known sources of harmonics include arc furnaces and welders, fluorescent lamps and static VAR compensators. Each of these nonlinear apparatus is discussed below.

Transformer saturation, i.e., the deviation from the linear relationship between the magnetic flux in iron and the magnetizing force, causes a nonsinusoidal excitation current to correspond with a sinusoidal applied voltage. The excitation current distortion contains mainly the third harmonic, but the fifth and the seventh order harmonics may also be large enough to produce visible distortion.

Transformers are also known to generate other harmonic currents (inrush currents) when re-energized after being switched-off. Because of the residual flux in the core, transformers will be driven into extreme saturation during the first seconds of operation. This effect gives rise to magnetizing currents of up to 10 times the rated current [4].

Electric machines generate harmonics as a result of the harmonic contents of the m.m.f. distribution. At a rotor slip s, an n-th order harmonic in the rotor m.m.f. induces an e.m.f. in the stator at a frequency equal to (n-s(n±1)) times the fundamental frequency [32]. Nonsymmetrical rotor windings are also known to cause harmonic distortion. In such a case, both positive and negative sequence currents will flow in the rotor, creating forward as well as backward rotating fields. The harmonic frequencies of stator e.m.f. induced by these fields are (1-2s) times the fundamental frequency. Variations of the magnetic reluctance of electrical machines caused by stator and rotor slots also generate harmonics, but these harmonics are not significant.

Arc furnaces and **arc welders** induce harmonics due to the nonlinear voltage-current characteristic of power arcs. These loads are usually modeled as harmonic current sources with the third, fifth, seventh and ninth order harmonics as the most prevalent components. The magnitudes of these harmonics vary continually due to the random nature of arc currents, especially during the melting phase.

Gaseous discharge lighting, such as fluorescent, mercury arc and high pressure sodium lamps, is a significant source of power system harmonics, particularly in metropolitan areas. The electrical characteristics of these lamps are quite nonlinear, thus giving rise to considerable levels of harmonic currents. The magnitudes of the third and fifth harmonic currents generated by typical fluorescent lamps are respectively on the order of 21% and 7% of the fundamental component.

Static VAR compensators, because of their fast response, high efficiency and low maintenance, are finding increasing use in improving power system voltage regulation and power factor correction [33]. These

compensators use thyristor-controlled reactors or capacitors, thus generating considerable amounts of harmonic distortion. The magnitudes of these harmonics depend on the delay angles of the SCRs. The dominant harmonic currents are of the third and fifth orders which can respectively reach 30% and 10% of the fundamental component.

2.2 Harmonic Effects

Harmonics may affect any of the four categories: power components (capacitors banks, transformers, electric machines, transmission lines), instrumentation (ripple control systems, protective devices, watthour meters), power efficiency and communication systems. Each of these categories will be discussed below.

2.2.1 Power Components

Shunt Capacitors. Capacitor impedance decreases with frequency. For this reason, capacitor banks act as "sinks" for harmonic currents. In a system with distributed harmonic sources, the harmonics will converge to the capacitor banks, and may result in fuse-blowing or capacitor failure. The total power loss in capacitor banks in the presence of harmonics is expressed by

$$P_{loss} = \sum_{n=1}^{\infty} C \, (\tan\delta)\omega_n V_n^2 \qquad (5)$$

where $(\tan\delta)$ is the loss factor, ω_n and V_n are the angular frequency and the rms value of the n-th harmonic voltage.

Capacitor banks, such as those used for power factor correction, can also form a resonant circuit with the rest of the system impedance at a frequency near a harmonic frequency. This can result in overvoltages

and excessive currents often leading to their destruction. Moreover, the total reactive power including the fundamental and harmonics should not exceed the rated reactive power.

Transmission Lines. The flow of harmonic currents in transmission lines causes additional power loss as given by

$$P_{loss} = \sum_{n=2}^{\infty} I_n^2 R_n \tag{6}$$

where R_n is the line resistance at the n-th harmonic frequency. it is noted that R_n increases with frequency due to skin effect.

The presence of harmonic voltages causes a rise in the line insulation stress, particularly in cable transmission. Since the peak voltage depends on the phase relationship between the harmonics and the fundamental, it is possible for the peak voltage to be higher than the rated value while the rms voltage is well within limits. The effect of high peak voltages shortens the life expectancy of transmission lines and cables.

Transformers. Voltage harmonics can cause transformers to be under higher insulation stress. This, however, is not a problem since transformers are insulated for much higher voltage levels. On the other hand, harmonic currents cause additional copper losses which result in increased heating. These losses are insignificant for the harmonic levels expected in distribution systems ($< 10\%$) [3]. However, these losses must be taken into account in converter transformers where the harmonic levels are much higher than 10%.

Electrical Machines. Additional power loss is the most serious effect of harmonics on a.c. machines. The capability of a machine to cope with extra losses will depend on the overall machine temperature

rise and local overheating. According to Ref. [34], supplementary heating alone can limit the voltage harmonic distortion for induction motors to 10%.

It is noted that in the presence of harmonics, the damper winding in synchronous machines carries current continuously. Therefore, these damper winding losses have to be taken into account in the design process, particularly if the generator is feeding large static converters. The effect of voltage harmonics on the mean torque is not significant for harmonic levels up to 20% [35]. However, pulsating torques caused by the interaction between fundamental and harmonic fluxes can possibly result in mechanical oscillations. Therefore, anticipated mechanical vibrations should be avoided.

2.2.2 Electric InstrumentS

Watthour Meters. Induction watthour meters, which are initially calibrated for pure sinusoidal voltages and currents, may lose their accuracy with distorted waveforms. Based on the results of recent studies [6], [36], the following conclusions are made:

(a) The frequency response curve of induction watthour meters shows relatively large registration errors for individual power harmonics at higher frequencies.

(b) Because of the meter nonlinearity, the simultaneous registration of multiple power harmonics is slightly different from the sum of registrations the power harmonic components would produce individually.

(c) For fair billing considerations, not only the magnitude but also the direction of power harmonic flow is of importance since the error sign is mainly determined by their relative directions.

(d) With a sinusoidal voltage waveform, the registration error is caused by the nonlinearity of the magnetic circuits, and is relatively small unless the third harmonic current component is large. In cases where both the voltage and current are distorted, the error is relatively large even for small voltage distortion factors.

Ripple Control and Carrier Current Systems. Ripple control systems, such as the one used for remote control of street lighting, operate in a frequency range of 290-1650 Hz. Thus, the presence of harmonics in power lines may cause signal blocking or maloperation of ripple relays [23]. The amplitude at which a voltage harmonic will affect the ripple relay is a function of the relay detection circuit.

Carrier current systems operate in the range of 5-10 kHz. It would appear that potentially interfering harmonics from nonlinear loads will be of a magnitude too low to cause problems in carrier systems. However, converters can be troublesome because of their voltage notches creating high frequency harmonics.

Protective Relays. Harmonics can degrade the operating characteristics of protective relays depending upon the design features and operation principle. Tests show that both electromechanical and static relay performances are affected by waveform distortion [7], [37]. In particular, the characteristics of overcurrent and overvoltage relays change dramatically in the presence of harmonics, and the operating torques of some electromechanical relays can be reversed at certain harmonic frequencies. Digital relay performance relying on zero crossings of signals can obviously be degraded by excessive harmonic content in the system.

2.2.3 Power Factor

Power factor represents a figure of merit of the character of power consumption. If the voltage and current are expressed by

$$v(t) = \sum_{n=1}^{\infty} \sqrt{2}\, V_n \sin(n\omega t + \alpha_n) \tag{7}$$

and

$$i(t) = \sum_{n=1}^{\infty} \sqrt{2}\, I_n \sin(n\omega t + \alpha_n + \phi_n), \tag{8}$$

then the power factor is given by the ratio of average power P to apparent power S, i.e.,

$$pf = \frac{P}{S} = \frac{\int_0^T v(t)\, i(t)\, dt}{V_{rms} I_{rms}} = \frac{\sum_{n=1}^{\infty} V_n I_n \cos(\phi_n)}{[(\sum_{n=1}^{\infty} V_n^2)(\sum_{n=1}^{\infty} I_n^2)]^{\frac{1}{2}}}. \tag{9}$$

Since the reactive power is defined by [38]

$$Q = \sum_{n=1}^{\infty} V_n I_n \sin(\phi_n), \tag{10}$$

then the apparent power S can be expressed by

$$S = (P^2 + Q^2 + D^2)^{\frac{1}{2}} \tag{11}$$

where D is an additional component designated as distortion power.

Under sinusoidal conditions, unity power factor can easily be achieved by placing a passive element (capacitor or reactor) in parallel with the load. However, power factor compensation is not straightforward when voltage and current waveforms are distorted. A passive network can improve the power factor by compensating the reactive power in (10), but unity power factor cannot be obtained because of the distortion power defined in (11).

2.2.3 Communication Systems

Most distribution system harmonic frequencies lie in the range used in commercial voice transmission (200 - 3500 Hz). Because of the great difference between the power levels of a distribution circuit (10^3-10^5W) and a telephone circuit (10^{-5}-10^{-3}W), the presence of harmonics may result in perceptible or even unacceptable telephone noise. Harmonic interference with communication systems is due to proximity and exposure of the communication circuits to the power network. Coupling between telephone and power circuits is through conduction, loop induction, longitudinal electrostatic or electromagnetic induction, with electromagnetic coupling as the dominant factor.

Telephone interference is often measured by the I.T product where I is the total rms current and T is the T(elephone) I(nfluence) F(actor) defined by [23]

$$TIF = \left[\sum_{n=1}^{\infty} (5nf\, C_n V_n^2) \right]^{\frac{1}{2}} / V_{rms} \qquad (12)$$

where C_n is the C-message weighting at the n-th harmonic frequency and f is the rated linear frequency. Transmission techniques such as underground cables and microwave links have minimized exposure of communication circuits to power harmonics. However, there are still cases where the pole line is shared by both power and telephone lines.

2.3 Methods of Reducing Harmonic Levels

In order to keep power system harmonics at acceptable levels, harmonic control may be required at particular harmonic sources, or on the power network in general. The principal reduction methods for large converters are harmonic cancellation and harmonic filtering. Several

other harmonic control methods are available but have not been adopted for large converters.

2.3.1 Harmonic Cancellation

Using this method, harmonic control takes place at the source itself through the cancellation of certain harmonics by increasing the converter pulse number p in the characteristic harmonic order equation given in (1). Harmonic cancellation involves the use of either transformers (for rectifiers) or specialized magnetics (for inverters) to phase-shift multiple converter units in order to obtain cancellation of some harmonics which are inherently present in the individual converter units.

As an example, Fig. 2 shows a twelve-pulse configuration consisting of two six-pulse phase-controlled rectifiers. The resultant a.c. current is given by the sum of the currents flowing in the Y-Y and Y-Δ transformers:

$$i(t) = \frac{4\sqrt{3}}{\pi} I_d\{\cos(\omega t) - \frac{1}{11}\cos(13\omega t) + \frac{1}{13}\cos(23\omega t) - \frac{1}{23}\cos(23\omega t)\ldots\}. \quad (13)$$

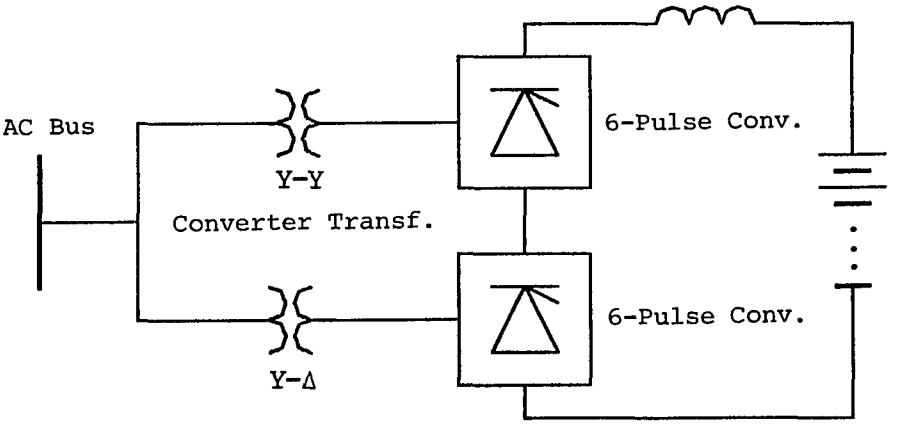

Fig. 2. Twelve-Pulse Converter Configuration.

The resulting current contains only harmonics of the order 12i±1. It is noted that the harmonic currents of the order 6k±1 (with k odd) circulate between the two converter transformers but do not penetrate the a.c. network. In practice, however, the cancellation is not perfect and these harmonics are found to be of the order of 15 - 25% of their full strength values [27].

An advantage of the harmonic cancellation technique is that cancellation takes place independently of the power system configuration. Harmonic cancellation is usually more economical for increasing a converter pulse number from 6 to 12, but becomes uneconomical for higher pulse numbers.

2.3.2 Harmonic Filtering

This reduction technique utilizes shunt filters which basically establish more or less short-circuit paths for the source harmonics, so that most of the harmonic currents do not enter the system network. in general, harmonic filters provide all or part of the reactive power required by phase-controlled rectifiers. The reactive power requirement usually determines the size of the filter bank.

An important factor to consider in filter design is the frequency-dependent impedance looking into the power network at the converter bus (driving point impedance). This impedance, Z_{pn}, will be in parallel with the filter impedance, Z_{fn}, as shown in Fig. 3. The resulting harmonic current flowing in the filter is given by

$$I_{fn} = \frac{Zpn}{Z_{pn} + Z_{fn}} I_n. \qquad (14)$$

If parallel resonance exists between the filter and supply impedance ($Z_{fn} + Z_{pn} \longrightarrow 0$) at a characteristic harmonic frequency, then from (14), it is clear that amplification of the harmonic current will occur and result in subsequent damage to the filter.

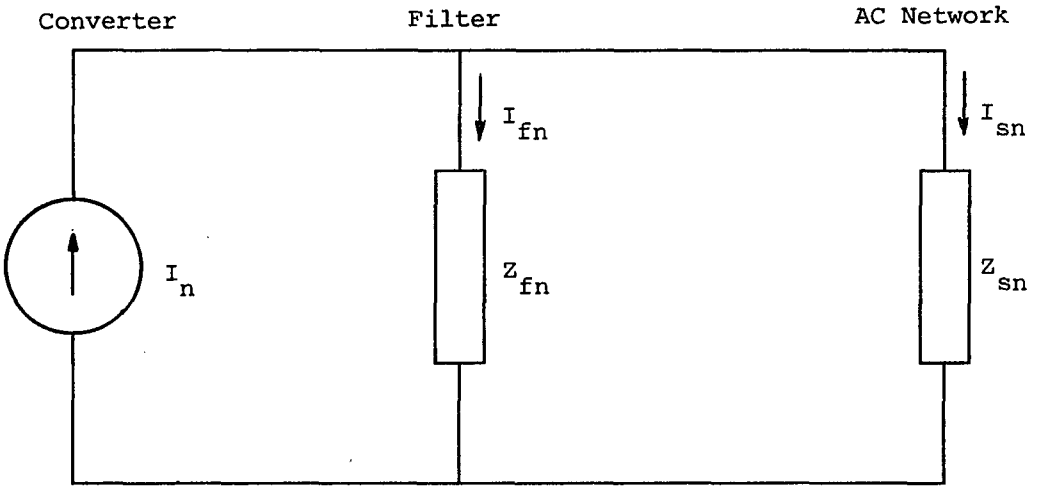

Fig. 3. Reduced Equivalent Circuit of Converter-Filter-Power Network.

Digital computer programs, which will be discussed in the next chapter, are readily available to compute the frequency-dependent driving point impedance. The filter bank should be designed without creating undesirable resonant conditions. If parallel resonance occurs at a source harmonic frequency, the total capacitance of the filter can be changed to avoid this condition. An alternative method is to increase the total impedance of the filter bank at the resonance frequency by adding a series damping resistor to the filter.

In large ac/dc power converter installations, two or more tuned filters are employed for the lower harmonics, and a high pass filter is used for the remaining higher-order harmonics. In smaller converter

stations, a high-pass damped filter may be sufficient for the harmonic suppression requirements.

2.3.3 Alternative Methods of Harmonic Elimination

Because of the complexity and cost of filters, there have been several attempts to achieve harmonic control by other means. Harmonic elimination is accomplished by magnetic flux compensation [39], current injection [40], pulse width modulation [41] and d.c. ripple injection [42].

Magnetic flux compensation is based on injecting a compensating current into a tertiary winding of the converter transformer. A filter removes the fundamental component from the waveform of the transformer secondary current obtained through a current transformer. The resulting current signal is then amplified and fed into the transformer tertiary winding in such a way to oppose the mmf produced by the secondary current harmonics. A disadvantage with this scheme is its inability to effectively remove the lower order harmonics without the need of a very high power feedback amplifier.

The current injection method requires an external harmonic current source which is added to the converter current. If the injected current is adjusted such that it is equal in magnitude but 180 out of phase with the converter current harmonic, then cancellation takes place. However, this method suffers from the need of an external harmonic generator and its synchronization to the supply's main frequency, as well as from its inability to nullify more than one harmonic order.

The pulse width modulation (PWM) technique for harmonic reduction is applicable only to inverters and has been successfully applied in

variable speed a.c. drives. PWM involves notching of the output voltage waveform in a manner so as to reduce or eliminate particular harmonic components by adjusting the width of the notches. Theoretically, all harmonics up to an arbitrary order can be eliminated. In practice, however, this is limited by the additional switching losses induced by the notches and the number of notches required per cycle.

Direct current ripple injection is an alternative method of current injection where, instead of using an external harmonic source, a square-wave current is fed from the rectifier d.c. output to the converter transformer through a feedback inverter. The feedback inverter is connected to the secondary windings of the converter transformer by two additional single-phase transformers and blocking capacitors. With phase and frequency adjustment of the injected current, a six-pulse rectifier configuration can be converted into a twelve-pulse converter system from the point of view of a.c. system harmonics.

3. METHODS OF PREDICTING HARMONIC LEVELS

Two main objectives for performing a harmonic analysis are to correct an existing harmonic problem and to estimate voltage distortion and current harmonics due to a new nonlinear load. Other objectives, such as identifying and locating a disturbing source [43], can probably be better achieved by field measurements. Typical existing problems which require harmonic analysis include equipment failure, excessive voltage distortion and interference with communication circuits. The objective is then to determine how to effectively suppress the particular harmonics creating the problem. When a major harmonic source is to be added to a power system, a harmonic study should be conducted to determine the resultant voltage distortion and harmonic current injected into the system. It is imperative that harmonic currents and voltages be kept at the lowest level possible to minimize their adverse effects on power system components.

The complexity and relatively high cost of accurate harmonic measurements [10], particularly on high voltage networks, has led to the development of analytical and computer models for the computation of harmonic levels. In general, a harmonic study includes decisions about the system model, orders of harmonics to be considered and the method of analysis.

This chapter is arranged in two parts. The first part deals with the harmonic modeling of various power system components including nonlinear loads. The second part describes the different methods for predicting harmonic levels and their advantages and limitations.

3.1 System Component Models

It is of great importance to use sufficiently accurate component models in harmonic studies. Most conventional components are represented by their equivalent impedances which are adjusted for each harmonic frequency. However, depending upon the method of harmonic analysis, nonlinear loads may be treated as piece-wise linear loads, harmonic current sources which depend on the voltage supply distortion, or simply constant harmonic current sources. A list of component models including linear and nonlinear loads are given in Table I.

Nonlinear Loads. One of the major harmonic sources in power systems is the three-phase line commutated ac/dc converter as mentioned in the previous chapter. Converters are usually modeled as constant harmonic current sources whose magnitudes are given by equations (2)-(4). A more complete description of harmonic current magnitudes as functions of delay and commutation angles is given in Ref. [23].

The converter phase currents can also be solved analytically in terms of the three-phase voltages. Each of the converter operating modes during every half cycle can be described by linear first-order differential equations. Then the currents can be solved in terms of applied voltage, circuit parameters, power, delay and commutation angles. Next, the Fourier series of these expressions can be found analytically, thereby obtaining the desired Fourier series of the converter current in terms of the Fourier series of the terminal voltages. This procedure is outlined in detail in Ref. [44].

Other harmonic sources such as static VAR compensators and fluorescent lamps can be treated as constant harmonic sources or can be modeled analytically in terms of the applied voltages [45], [46]. Arc

TABLE I. SYSTEM COMPONENT MODELS

Nonlinear Load	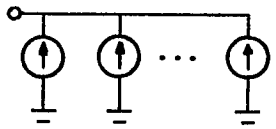
Linear Load	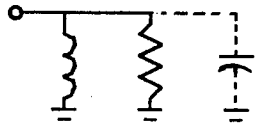
Transmission Line	
Inductor, Capacitor	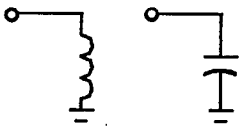
Induction Machine	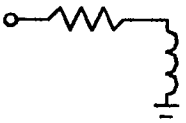
Synchronous Generator	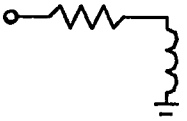
Transformer	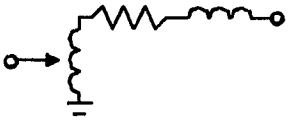
Equivalent of Remaining Network	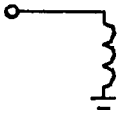

furnaces and welders are variable loads whose voltage and current characteristics must be approximated by average values in order to be incorporated in steady-state harmonic analysis. Transformers and electric machines are harmonic producers, but they are generally treated as

linear components since the harmonics they produce are relatively small compared to those produced by solid-state power converters.

Linear Loads. It is difficult to model linear system loads since the exact composition is often unknown. It is suggested [12] that, lacking information on the specific load composition at a bus, the load be modeled as a shunt resistance in parallel with a shunt inductance or capacitance. These linear elements are selected to account for the active and reactive power, P and Q, at the fundamental angular frequency ω, i.e.,

$$R = \frac{V_1^2}{P}, \qquad L = \frac{V_1^2}{\omega Q}, \qquad C = \frac{Q}{V_1^2 \omega}. \tag{15}$$

If the linear loads are distributed, they may be divided in two equivalent lumped loads at the two ends of the line section over which they are distributed.

Transmission Lines and Cables. In line frequency analysis, skin effect has to be taken into consideration. Other than this, line equivalent circuit for harmonics is basically the same as for the power frequency. Considering a frequency range of interest of up to 3 kHz (50-th order harmonic for a base of 60 Hz), π-equivalent circuits should be used for overhead lines longer than 3 miles and for underground cables longer than 0.5 miles.

It is, however, recognized that even though the -equivalent circuit provides accurate results at the line terminals, it hides other important information. Of particular concern is the maximum harmonic current or voltage that may occur at points other than the line terminals due to standing wave phenomena. This topic will be explored in detail in

chapter 5.

Capacitors and **Inductors.** Capacitors and inductors are treated as pure circuit elements with fixed capacitance and inductance. Therefore, the impedance of shunt capacitors is inversely proportional to the frequency, and the impedance of inductors is directly proportional to the frequency.

Induction Machines. The standard model of a three-phase induction machine is shown in Fig. 4(a). For harmonic purposes, the magnetizing inductance L_m is often ignored, leaving a simple equivalent loop circuit shown in Fig. 4(b). For the n-th harmonic frequency, the slip S at rated speed is reduced to

$$S = \frac{n\omega_s \pm \omega_r}{n\omega_s} \simeq 1 \pm \frac{1}{n} \tag{16}$$

Therefore, the slip approaches unity as n increases. For this reason, it is suggested [12] that, as a first approximation, induction motors be modeled by their equivalent locked rotor elements. Furthermore, the reactive term is much more dominant than the series resistance so that the model is reducible to a pure inductive shunt.

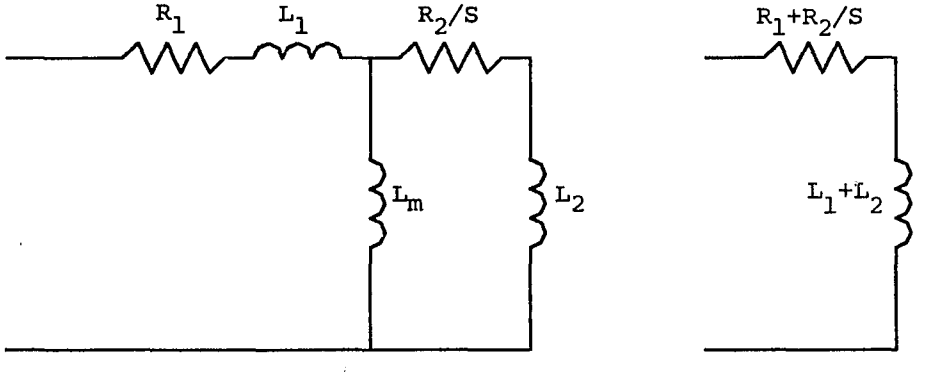

Fig. 4. Induction Motor Model: (a) Exact and (b) Approximate.

Synchronous Generators. The reluctance path of an a.c. generator viewed by harmonic fluxes is effectively the same as that experienced by negative sequence fluxes of the power frequency. Thus, the effective inductance experienced by the harmonic currents is the negative sequence inductance, which is the average of the direct-axis and quadrature-axis subtransient inductances [21]. If the equivalent resistances representing the core and damper winding losses are neglected, the generator can be satisfactorily represented by its negative sequence reactance in series with the stator winding a.c. resistance.

Transformers. Transformers are best modeled with turn-to-turn distributed inductances and capacitances. These devices have widely varying frequency-dependent impedances with several resonant frequencies. Fortunately, these frequencies are reported to be considerably beyond the normal range of interest in harmonic analyses (between 7 kHz and 15 kHz) [47].

The most common transformer model used in harmonic studies is that shown in Table I where the shunt impedance is ignored and the leakage inductance is assumed to be constant. The series resistance, however, is frequency-dependent due to proximity and skin effect. The variation of this resistance with frequency is found in Ref. [43]. Finally, the phase shift of the transformer model is needed to represent the wye-delta transformer connection.

Equivalent of Remaining Network. Generally, power system connections make it unfeasable to have a complete representation of the entire power network. Complete representation of all components located in the region of interest is necessary to obtain accurate results. However,

the remaining network outside the region of interest has to be approximated by some Thevenin equivalent. It is suggested [48] to represent any remaining network connected to an outside bus (which is defined as a bus on the border of the region of interest) by the short-circuit negative sequence reactance at the power frequency times the harmonic order under consideration.

3.1 Harmonic Analysis Methods

Presently, three different computer methods of various complexity are available for power system harmonic analysis; namely, the nonlinear time domain analysis, the nonlinear frequency domain analysis and the linear frequency domain analysis. All these methods employ the same component models except for the nonlinear components. A brief description of each of these methods is presented in the following sections, outlining the differences between these methodologies and the results that can be expected.

3.3.1 Nonlinear Time Domain Analysis

Time domain simulation offers a direct relationship with the actual physical behavior of the power system. In this method, the converter is modeled as a set of ideal switches with a linear load, i.e., a piecewise linear element [49]. For each operation mode of the switches, the network differential equations are formulated in standard state-variable form

$$[\dot{X}(t)] = [A]\ [X(t)] + [B]\ [U(t)] \tag{17}$$

where [X(t)] represents the instantaneous bus voltages and currents, [U(t)] is the generator supply voltages, and [A] and [B] are constant matrices which depend on the linear network elements and operation mode.

A numerical integration of (17), starting from a set of initial conditions results in the voltage and current waveforms. The results include the full transient performance of the power network from the initial point to the steady state which is reached after a large number of cycles. The harmonic voltage and current magnitudes are then found by running the resulting waveforms through a Fast Fourier Transform (FFT).

If the transient state is not of interest, an appropriate choice of the initial conditions generally leads to a faster solution. Several techniques for accelerating the convergence have been explored [50], [51], but the solution time still remains lengthy. In addition, the several switchings of the SCRs per cycle impose a small integration step size. Therefore, the time domain simulation is limited to the analysis of small systems.

3.2.2 Nonlinear Frequency Domain Analysis

Xia and Heydt [14], reformulated the Newton-Raphson power flow algorithm to accomodate nonlinear loads. Before including harmonics in the power flow program, it is necessary to know in advance the steady-state voltage-current relationship at nonlinear load buses, from which a Fourier series expression of the load current is obtained in terms of load harmonic voltage and nonlinear load parameters.

The concept of harmonic load flow can, perhaps, be more clearly understood by comparing it to the conventional power flow [52]. The fundamental frequency Newton-Raphson algorithm is based on the reduction of active and reactive power mismatch to less than some prescribed tolerance at the system buses. The partitioned matrix formulation of

the problem is

$$\begin{bmatrix}[\Delta P]\\ [\Delta Q]\end{bmatrix} = \begin{bmatrix}[\partial P/\partial \delta] & [\partial P/\partial V]\\ [\partial Q/\partial \delta] & [\partial Q/\partial V]\end{bmatrix}\begin{bmatrix}[\Delta \delta]\\ [\Delta V]\end{bmatrix} \tag{17}$$

where $[\Delta P]$ and $[\Delta Q]$ are the calculated active and reactive incremental power at each bus (except the swing bus), $[\Delta \delta]$ and $[\Delta V]$ are the desired voltage angle and magnitude correction (except at the swing bus).

In a harmonic power flow, network voltages and currents are represented by the Fourier series up to a specified order of interest N. Harmonic bus voltages and angles are unknown for which additional equations are needed. The additional equations are based on Kirchhoff's current law for each harmonic and the conservation of apparent voltamperes at nonlinear buses. The specified quantities include: (1) the total active power at all buses except the swing bus, (2) the total reactive power at all linear load buses except the swing bus, and (3) the total reactive voltamperes at all nonlinear load buses.

The resulting matrix formulation of harmonic load flow is given by

$$\begin{bmatrix}[\Delta W]\\ [\Delta I_1]\\ \vdots\\ [\Delta I_N]\end{bmatrix} = \begin{bmatrix}[0] & [J_1] & \cdots & [J_N]\\ [H_1] & [YG_1^1] & \cdots & [YG_1^N]\\ \vdots & \vdots & & \vdots\\ [H_N] & [YG_N^1] & \cdots & [YG_N^N]\end{bmatrix}\begin{bmatrix}[\Delta \Phi]\\ [\Delta V_1]\\ \vdots\\ [\Delta V_N]\end{bmatrix} \tag{18}$$

where

$[\Delta W]$ = active and reactive power balance at all buses

$[\Delta I_1]$ = fund. real and imaginary current balance at nonlinear buses

$[\Delta I_n]$ = n-th harmonic active and reactive current balance at all buses

$[\Delta V_n]$ = n-th harmonic voltage magnitude and angle at all buses

$[\Delta \Phi]$ = state variable mismatch for each nonlinear load

$[J_n]$ = conventional Jacobian matrix at n-th harmonic frequency

$[H_n]$ = partial derivative of nonlinear load currents with respect to nonlinear device state variables

$[YG_j^n] = [Y_n^n] + [G_n^n]$ when n=j, or $[G_j^n]$ when $n \neq j$.

Herein,

$[Y_n^n]$ = partial derivative of injected n-th harmonic current with respect to n-th harmonic bus voltage as derived from the system admittance matrix

$[G_j^n]$ = partial derivative of n-th harmonic current with respect to the j-th harmonic applied voltage as determined by the nonlinear load characteristic.

The set of nonlinear equations in (18) is solved in a manner analogous to the conventional load flow problem. It was noted [14] that the convergence rate to a solution is slower for the harmonic power flow than for the fundamental frequency power flow due to the difficulty in choosing intial values close to the final solution for the harmonic frequencies. In addition, only nonlinear load models of converters [14] and gaseous discharge lamps [45] are available at present. Due to these limitations, the nonlinear frequency domain method has been limited to balanced and relatively small systems.

3.2.3 Linear Frequency Domain Analysis

An alternative approach to power system harmonic analysis is made available by treating the nonlinear loads as constant harmonic current sources (this method is sometimes referred to as the current injection method). These current harmonics are functions of their fundamental in both magnitude and phase angle, and are therefore independent of the

voltage waveform.

For simple circuit configurations, a harmonic analysis can be done manually. The most simple circuit configuration is shown in Fig. 5 where a large industrial converter with a power factor correction capacitor is connected to a substation transformer. Let the source-transformer impedance be given by

$$Z = R + j\omega L \tag{19}$$

then the resonant frequency, which should not be near the frequency of the injected harmonic currents, is given by

$$f = \frac{1}{2\pi}\left[\frac{L - R^2C}{CL^2}\right]^{\frac{1}{2}}. \tag{20}$$

The n-th harmonic voltage at the capacitor bank is expressed by

$$V_n = I_n \left|\frac{R + j\omega L}{1 - \omega^2 LC + j\omega CR}\right|, \tag{21}$$

and the injected current into the utility supply is

$$I_n^s = V_n\left|1/(R + j\omega L)\right|. \tag{22}$$

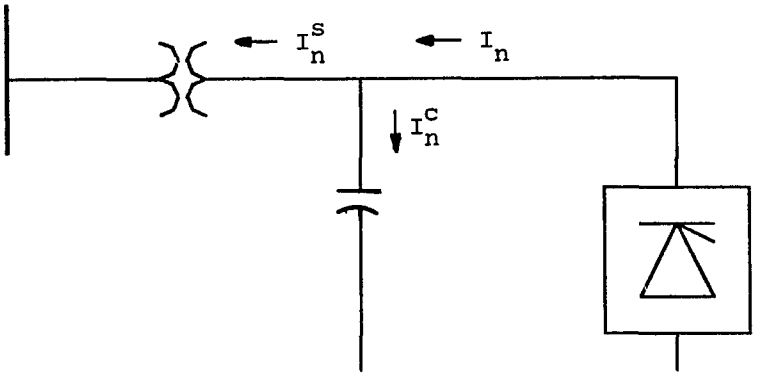

Fig. 5. Simplest Circuit for Harmonic Analysis.

More complex circuits with multiple buses and distributed nonlinear

loads are better analyzed by computer. Here, the superposition principle can be used where harmonics of different orders are treated separately. To illustrate, consider an m-bus power system where harmonic currents are injected at buses through m as shown in Fig. 6. Then the network equation using the bus impedance matrix at the n-th harmonic frequency can be written as

$$\begin{bmatrix} V_n^1 \\ V_n^2 \\ \vdots \\ V_n^{\ell} \\ \vdots \\ V_n^m \end{bmatrix} = \begin{bmatrix} Z_n^{11} & Z_n^{12} & \cdots & Z_n^{1m} \\ Z_n^{21} & Z_n^{22} & \cdots & Z_n^{2m} \\ \vdots & \vdots & \ddots & \vdots \\ Z_n^{m1} & Z_n^{m2} & \cdots & Z_n^{mm} \end{bmatrix} \begin{bmatrix} 0 \\ 0 \\ \vdots \\ I_n^{\ell} \\ \vdots \\ I_n^m \end{bmatrix}. \tag{23}$$

Techniques for assembling the impedance matrix [Z], i,j=1,2,...,m, are readily available in Ref. [21].

From (23), the n-th harmonic voltage at bus k and the harmonic current flowing from bus i to bus j are respectively given by

$$V_n^i = \sum_{h=\ell}^{m} Z_n^{ih} I_n^h \tag{24}$$

and

$$I_n^{ij} = \{V_n^i - V_n^j\}/Z_n^{ij}. \tag{25}$$

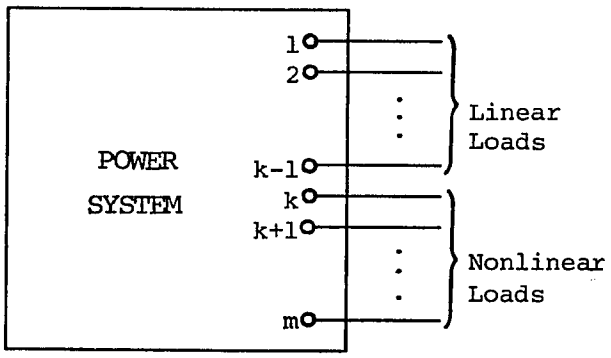

Fig. 6. Power System with Multiple Nonlinear Loads.

It is evident that the resultant n-th harmonic voltage caused by multiple harmonic sources is not only dependent on the magnitudes of the current harmonics of the same order but also on their phase angles. These phase angles can be found from the local phase relationships between the current harmonics and their fundamentals, along with the phase relationships between the fundamentals at the harmonic source buses.

The linear approach offers computational efficiency while giving up some accuracy which represents the primary limitation of this method. However, recent research [43] has shown that the current injection method is adequate where voltage distortion factor is less than 10%, which is generally the case. This method has been applied successfully to real-life power systems [11], [22] and due to its computational efficiency, it is the most widely used to date.

4. PROBABILISTIC MODELING OF POWER SYSTEM HARMONICS

Power system harmonic analysis has been conventionally conducted in a deterministic framework with input parameters controlling the current harmonics represented by fixed values. Any random changes in the harmonic current injection are therefore not reflected in the harmonic current flows and resulting harmonic voltages. However, it has been recognized [16] that power system voltage and current harmonics are time-variant due to stochastic or deterministic changes in the operating mode of nonlinear loads, such as arc furnaces and variable speed drives. Measurements show that the variation of harmonic levels in most networks is often so erratic that a single reading can be misleading.

With a random current injection, the highest possible harmonic levels are usually used in deterministic programs. This practice is referred to as the "worst case method" [53]. The resulting harmonic currents and voltages may occur very rarely (e.g., for only a few seconds of the day) and, therefore, may be of minor significance to harmonic assessment studies. Consequently, statistical models of harmonic current injection and propagation are highly desirable for a more realistic prediction of harmonic levels [15], [16], [27]. Probabilistic evaluations take into account the variations of harmonic currents and provide more details than deterministic assessements. The extra information will allow filters and power components in general to be more effectively and economically designed.

A number of theoretical studies were dedicated to the summation of random phasors with reference to harmonics [54]-[56]. However, these analyses are based on the assumption that the harmonic amplitudes and/or

their phase angles are independent and uniformly distributed. In Ref. [57], the randomness of injected harmonic currents is traced back to changes in the variable parameters governing the operating modes of nonlinear loads. Other publications have investigated the probability characteristics of harmonic injection generated by some specific nonlinear loads (NLs), including traction drives [58], electric vehicle battery chargers [17], TV receivers and light dimmers [18], and d.c. drives [19].

In the most general case, the NLs may have different ratings and operating modes which are either deterministic or non-deterministic in nature. In addition, the configuration or switching state of NLs connected to a common bus may be fixed, deterministically, or randomly varying with time.

In this chapter, a probabilistic model for harmonic analysis [59] is proposed where injected harmonic currents may be partly deterministic and partly random. A classification of harmonic generators, depending on their operating mode and switching state, is given first. Then, based on some reasonable assumptions, a general procedure is presented to a harmonic current injection which is partly deterministic and partly random for a bus having NLs of different categories. This is followed by a probabilistic model of the harmonic current propagation and the resulting harmonic voltages. The procedure is demonstrated by a detailed example which illustrates the probability aspects of power system harmonics. Lastly, potential applications of the probabilistic model are also considered.

4.1 Classification of Nonlinear Loads

In general, a distribution bus has nonlinear loads of different types of nonlinearity, operational modes and ratings. Some loads, once switched on, operate steadily (fluorescent lamps), others vary slowly and deterministically with time (battery chargers), while the rest are nondeterministic in nature (arc welders). Furthermore, the load switching state (i.e., the configuration of NLs in service) may also vary deterministically or randomly.

For each type of the NLs, let the statistical data of the random variables (parameters governing the operational modes and switching state of the NLs) be known. These statistical data may be determined by recording a large volume of information regarding the changes of the random variables for a sufficiently long period of time. In general, it is desirable to know the time interval of the day when the highest harmonic levels occur. Therefore, it is suggested to divide the daily (or weekly) cycle into a finite number of intervals whose durations may be of the order of minutes or hours, and define PDFs of the random variables at each time interval.

In each time interval, the nonlinear loads will generate currents which can be divided into four categories:

1. a deterministic number of deterministic currents (DNDC),
2. a random number of constant currents (RNCC),
3. a constant number of random currents (CNRC), and
4. a random number of random currents (RNRC).

In general, a distribution bus contains nonlinear loads of all of the above categories. At any instant, the total harmonic current injected at that bus is a summation of a deterministic and a random

harmonic current component. The total probability density function of the random harmonic component is derived in the following section.

4.2 Probability Distribution of Harmonic Injection

Before modeling a harmonic current injection deterministically and probabilistically, a number of assumptions must first be made:

1. the nonlinear loads vary independently from each other,
2. the probability characteristics of the randomly varying NLs are readily available,
3. the rate of change in the number of nonlinear loads in service is low relative to the random change in the operating mode of NLs,
4. both the line and equivalent linear load impedances are time-invariant,
5. the distribution system is symmetrical and in balanced operating condition, consequently, limiting the analysis to the single-phase case, and
6. the system is operating in a quasi-steady state condition (the operating modes of the NLs vary sufficiently slow such that the resulting electrical transients are negligible).

The first assumption is somewhat questionable since there may be a correlation between the operating mode variations and switching states of the nonlinear loads (e.g., the sequence of operations in a steel mill or any process line). In general, however, these correlations are not well defined. Concerning the second assumption, statistical data for nonlinear loads are rare at the present time, so that the PDFs for most loads are not readily available. But the need for such important information has been repeatedly voiced [16]. It is therefore expected that

these statistical data will be available in the near future considering that suitable instrumentation to record such data is being developed [60]. The remaining assumptions are made primarily to reduce the complexity of the problem.

Consider the load arrangement of a distribution feeder in Fig. 7, where the load units are numbered in each nonlinear load category. Note that the linear load (LL) may also include capacitors for power factor correction. The total n-th order harmonic current phasor at any time is given by

$$I_n(t) = \sum_{m=1}^{4} I_{mn}(t) \tag{27}$$

with

$$I_{1n}(t) = \sum_{i=1}^{g} I_{1ni}(t) \tag{28}$$

$$I_{2n}(t) = \sum_{i \epsilon S_h} I_{2ni}(t) \tag{29}$$

$$I_{3n}(t) = \sum_{i=1}^{k} I_{3ni}(t) \tag{30}$$

and

$$I_{4n}(t) = \sum_{i \epsilon S_\ell} I_{4ni}(t) \tag{31}$$

where $I_{mni}(t)$ denotes the n-th harmonic current injected by load unit i of NL category m (all injected currents must be defined relative to a common phase reference). S_h and S_ℓ will be further defined in this section.

Equation (27) shows the n-th harmonic current composed of four components. Only the first component, $I_{1n}(t)$, is deterministic in nature, so that the probability aspect applies exclusively to the three remaining components defined in (29)-(31). The probability character-

istics of each current component will be found separately, from which the PDF of the total random current can then be deduced.

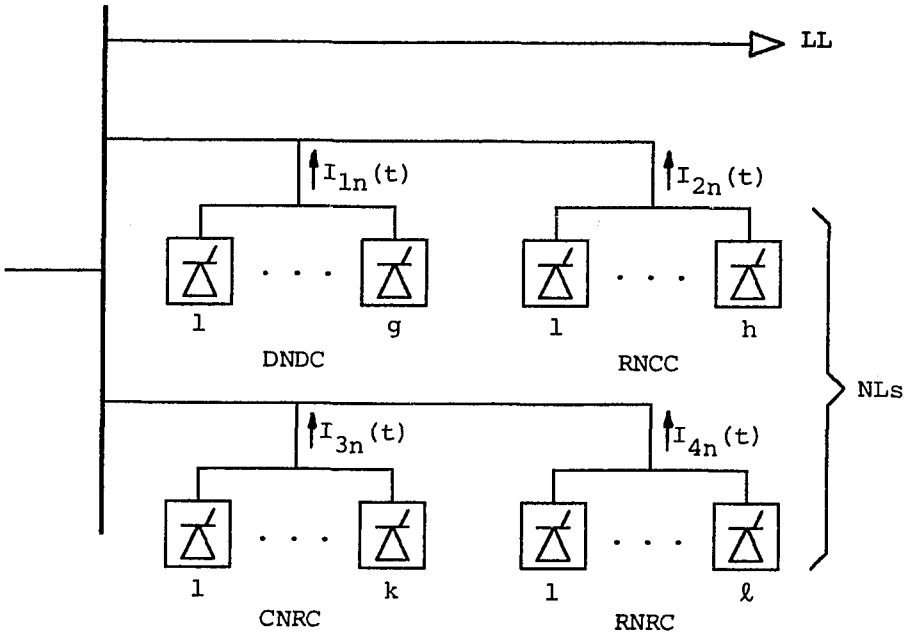

Fig. 7. Load Composition.

A two-dimensional random vector can be described by either the joint density function or the marginal density functions of its real and imaginary parts (x-y projections). In this paper, the latter description is chosen because the convolution process can be readily applied in obtaining the distribution of the summation of real random variables. Hence, a time-dependent complex n-th harmonic current generated by load unit i of NL category m will generally be written as

$$I_{mni}(t) = X_{mni}(t) + j\, Y_{mni}(t).$$

In the derivations that follow, both the real part X_{mni} and imaginary part Y_{mni} of each harmonic current in a time interval will be denoted by W_{mni} unless otherwise stated.

4.2.1 Sum of Random Number of Constant Currents

Define the sample space S_h to be the collection of all possible NL configurations in the RNCC category, i.e.,

$$S_h = \{\tau_1, \tau_2, \ldots, \tau_{h'}\}$$

where h' may assume a value between 2^h (if all h NLs are different from each other) and h+1 (if all h NLs are identical). The symbol τ_j designates some switching state of the RNCC load category. The probabilities associated with each switching state are given by

$$P\{\tau_j\} = p_{\tau_j}, \qquad j=1,2,\ldots,h'.$$

Therefore, S_h constitutes a probability space of all possible switching states of the RNCC load category, and the random variables X_{2n} and Y_{2n} can be defined in S_h to associate respectively the real and imaginary parts of the resulting harmonic current with each τ_j:

$$W_{2n}(\tau_j) = w_j, \quad w=x,y.$$

where w_j is the sum of real (imaginary) parts of the n-th harmonic currents generated by the energized NLs designated by τ_j. Recognizing the discrete nature of τ_j, the PDF of the x-y projections of the current $I_{2n}(t)$ given in (29) is

$$P_{W_{2n}}(w_j) = p_{\tau_j}, \quad j=1,2,\ldots,h'. \tag{32}$$

4.2.2 Sum of Constant Number of Random Currents

In this category, the harmonic currents change randomly whereas the number of harmonic sources, k, is constant. Let α_i, i=1,2,...k, represent the varying parameter (e.g., firing angle in case of phase-controlled rectifiers) governing the random operating modes, and assume the PDF of α_i, $p_{\alpha_i}(\alpha)$, for each NL of this category to be known.

Considering that the x-y projections of a harmonic current as func-

tions of the variable parameter can generally be deduced, let

$$X_{3ni} = F_{3ni}(\alpha_i)$$

and

$$Y_{3ni} = G_{3ni}(\alpha_i)$$

be known. Then the PDFs of X_{3ni} and Y_{3ni} are given by [61]

$$p_{W_{3ni}}(w) = p_{\alpha_i}[H_{3ni}^{-1}(w)]\left|dH_{3ni}^{-1}(w)/dw\right|, \qquad (W,H) = (X,F),(Y,G) \qquad (33)$$

where H_{3ni}^{-1} represents the inverse function of H_{3ni}. It is pointed out that equation (33) applies only when F_{3ni} and G_{3ni} are strictly monotonous. If this is not the case, equation (33) can still be applied to several intervals of α_i where F_{3ni} and G_{3ni} are strictly monotonous in each interval. The PDFs in the individual intervals are then added at the corresponding values of X_{3ni} and Y_{3ni}.

Considering equation (30), the PDF of the real or imaginary part of $I_{3n}(t)$ is

$$p_{W_{3n}} = p_{W_{3n1}} * p_{W_{3n2}} * \cdots * p_{W_{3nk}} \qquad (34)$$

where the asterisk represents the standard convolution integral. It is noted that the mean and variance of the resulting distribution of equation (34) can be computed from

$$\mu_{W_{3n}} = \sum_{i=1}^{k} \mu_{W_{3ni}}$$

and

$$\sigma^2_{W_{3n}} \quad \sum_{i=1}^{k} \sigma^2_{W_{3ni}}$$

where $\mu_{W_{3ni}}$ and $\sigma^2_{W_{3ni}}$ respectively represent the mean and variance of the harmonic current projection generated by the i-th nonlinear load. These parameters are defined by

$$\mu_{W_{3ni}} = \int_{-\infty}^{\infty} w\, p_{W_{3ni}}(w)\, dw \tag{35}$$

and

$$\sigma^2_{W_{3ni}} = \int_{-\infty}^{\infty} (w - \mu_{W_{3ni}})^2 p_{W_{3ni}}(w)\, dw\,. \tag{36}$$

In particular, if the nonlinear loads of this category are identically distributed and k is sufficiently large, the central limit theorem strongly suggests that $p_{W_{3n}}(w)$ approaches a Gaussian density function given by [61]

$$p_{W_{3n}}(w) = \frac{1}{\sigma_{W_{3ni}}\sqrt{2\pi k}} \exp\left[\frac{w - k\mu_{W_{3ni}}}{2k\sigma^2_{W_{3ni}}}\right] \tag{37}$$

where $\mu_{W_{3ni}}$ and $\sigma^2_{W_{3ni}}$ represent the mean and variance of a single load.

4.2.3 Sum of Random Number of Random Currents

The final current category to be considered is given in (31) where both $I_{4ni}(t)$, i =1,2,..., and the load switching state are random variables. As in the CNRC case, let β_i be the random variable governing the operating mode of the i-th nonlinear load of this category with a PDF denoted by $p_{\beta_i}(\beta)$.

The PDF of the real or imaginary part of the current generated by the i-th nonlinear load is computed in the same fashion as for the CNRC category by equation (33), where the subscripts of W and H have to be modified from 3ni to 4ni to refer to the RNRC category.

Now, let the sample space of all possible NL configurations of the RNRC category be designated by

$$S_\ell = \{\nu_1, \nu_2, \ldots, \nu_{\ell'}\}$$

where ν_j represents some switching state of the RNRC category and ℓ' assumes a value between 2^ℓ (if all ℓ NLs are different from each other)

and $\ell+1$ (if all ℓ NLs are identical). Supposing the probabilities of the switching states ν_j, j=1,2,...ℓ', to be known, then

$$P\{\nu_j\} = p_{\nu_j}, \qquad j=1,2,\ldots,\ell'.$$

Since the rate of change in the load switching state is assumed to be low relative to the change in the operating mode, then, given ν_j, finding the PDFs of the x-y projections of the total current in switching state ν_j is identical to finding the total PDFs for the CNRC load category in the previous subsection. Thus, the conditional PDF, $p^{j}_{W_{4n}}(w)$,of the real or imaginary part of the total n-th harmonic current generated by the NLs in each of the switching states can be computed as in (34) resulting in the PDFs of the x-y projections of $I_{4n}(t)$ for all possible switching states as follows:

$$p_{W_{4n}}(w) = \sum_{j=1}^{\ell'} p_{\nu_j}\, p^{j}_{W_{4n}}(w) \tag{38}$$

4.2.4 Resultant n-th Harmonic Current Injection

The total n-th harmonic current injected is composed of a deterministic portion and a random part. The random part itself is a summation of three terms whose probabilistic models have already been derived. Furthermore, since these terms are considered to be independent of each other, both the real and imaginary parts of the total n-th harmonic random current are given by

$$p_{W_n} = p_{W_{2n}} * p_{W_{3n}} * p_{W_{4n}} \tag{39}$$

where $p_{W_{2n}}(w)$, $p_{W_{3n}}(w)$ and $p_{W_{4n}}(w)$ are respectively taken from equations (32), (34) and (38).

Noting that the magnitude of I_n is found from $|I_n| = (X_n^2 + Y_n^2)^{\frac{1}{2}}$, the PDF of $|I_n|$ can be computed stepwise as follows:

1. Find the PDF of X_n^2 and Y_n^2 using

$$p_{W_n^2}(w) = \{p_{W_n}(\sqrt{w}) + p_{W_n}(-\sqrt{w})\}/2\sqrt{w}. \tag{40}$$

2. Measurements show that X_n^2 and Y_n^2 of the high frequency harmonic currents (greater than or equal to the fifth order) are practically independent [58]. This can be recognized from the fact that any small changes in the fundamental components causes very eratic changes in the higher order components. The probability density function of the sum X_n^2 and Y_n^2 can be approximated by

$$p_{X_n^2+Y_n^2} = p_{X_n^2} * p_{Y_n^2}. \tag{41}$$

3. Noting that $|I_n|$ is the square root function of $X_n^2 + Y_n^2$, the PDF of $|I_n|$ is computed by using

$$p_{|I_n|}(i) = 2(i)\ p_{X_n^2+Y_n^2}[(i)^2]. \tag{42}$$

The mean and variance of $|I_n|$ are computed from (35) and (36) after replacing w and $p_{W_{3ni}}$ by $|I_n|$ and $p_{|I_n|}$.

The expression for $I_{1n}(t)$ in (28) and the PDFs in (39) and (42) provide a complete model of the n-th harmonic current injection at each bus containing nonlinear loads.

4.3 Probability Distribution of Harmonic Propagation

The effect of nonsinusoidal voltage on harmonic current injection in converter installations has been analyzed for steady-state conditions [44]. To attempt to incorporate similar considerations in random situations would lead to an unacceptable degree of complication. Furthermore, the effect of voltage distortion for most nonlinear loads is of secondary order if the voltage distortion factor is less that 10% [43].

In the following, the injected harmonic currents are therefore assumed to be independent of the voltage waveform.

An m-bus power system where harmonic currents are injected at buses ℓ through m as shown in Fig. 6, can be described by an m-th order set of linear complex algebraic equations for each harmonic order under consideration. The deterministic part of the n-th harmonic bus voltages and currents are computed by equations (25) and (26).

To find the PDFs of the real and imaginary parts of the random components of $V_n^k(t)$ and $I_n^{ik}(t)$, let

$$V_n^k = Q_n^k + j\, R_n^k,$$

$$I_n^{ik} = X_n^{ik} + j\, Y_n^{ik}$$

and

$$Z_n^{ik} = S_n^{ik} + j\, T_n^{ik}.$$

Then the real and imaginary parts of V_n^k and I_n^{ik} can be expressed as

$$Q_n^k = \sum_{i=\ell}^{m} (S_n^{ik} X_n^i - T_n^{ik} Y_n^i), \tag{43}$$

$$R_n^k = \sum_{i=\ell}^{m} (S_n^{ik} Y_n^i + T_n^{ik} X_n^i), \tag{44}$$

$$X_n^{ik} = \{S_n^{ik}(Q_n^i - Q_n^k) + T_n^{ik}(R_n^i - R_n^k)\}/\{(S_n^{ik})^2 + (T_n^{ik})^2\} \tag{45}$$

and

$$Y_n^{ik} = \{S_n^{ik}(R_n^i - R_n^k) - T_n^{ik}(Q_n^i - Q_n^k)\}/\{(S_n^{ik})^2 + (T_n^{ik})^2\}. \tag{46}$$

Noting that the probability density functions of the x-y projections of $I_n^k(t)$ have already been obtained by equation (39), and considering that X_n^{ik} and Y_n^{ik} are practically independent for higher order harmonics, the PDFs of Q_n^k, R_n^k, X_n^{ik} and Y_n^{ik} in (43)-(46) are respectively given by

$$p_{Q_n^k} = C_1\, p_{X_n^l}\left(\frac{x}{S_n^{lk}}\right) * \ldots * p_{X_n^m}\left(\frac{x}{S_n^{mk}}\right) * p_{Y_n^l}\left(\frac{-y}{T_n^{lk}}\right) * \ldots * p_{Y_n^m}\left(\frac{-y}{T_n^{mk}}\right), \tag{47}$$

$$p_{R_n}^{k} = C_1 \; p_{X_n}^{1}\left(\frac{x}{T_n^{1k}}\right) * \ldots * p_{X_n}^{m}\left(\frac{x}{T_n^{mk}}\right) * p_{Y_n}^{1}\left(\frac{y}{S_n^{1k}}\right) * \ldots * p_{Y_n}^{m}\left(\frac{y}{S_n^{mk}}\right), \tag{48}$$

$$p_{X_n}^{ik} = (C_2 C_3)^2 \; p_{Q_n}^{i}\left(\frac{q}{C_2}\right) * p_{Q_n}^{k}\left(\frac{-q}{C_2}\right) * p_{R_n}^{i}\left(\frac{r}{C_3}\right) * p_{R_n}^{k}\left(\frac{-r}{C_3}\right) \tag{49}$$

and

$$p_{Y_n}^{ik} = (C_2 C_3)^2 \; p_{Q_n}^{i}\left(\frac{-q}{C_3}\right) * p_{Q_n}^{k}\left(\frac{q}{C_3}\right) * p_{R_n}^{i}\left(\frac{r}{C_2}\right) * p_{R_n}^{k}\left(\frac{-r}{C_2}\right) \tag{50}$$

where

$$C_1 = \prod_{i=1}^{m} 1/|S_n^{ik} T_n^{ik}|, \quad C_2 = S_n^{ik}/\{(S_n^{ik})^2 + (T_n^{ik})^2\}, \quad C_3 = T_n^{ik}/\{(S_n^{ik})^2 + (T_n^{ik})^2\}.$$

From the above probability density functions, the PDF of the n-th harmonic voltage magnitude at any bus can be obtained by the same procedure described in (40)-(42). The same arguments hold for the harmonic current propagations.

4.4 Computational Methods

A method to compute a PDF composed of a convolution of several components, $p_i(w)$, $i=1,2,\ldots,N$, as in equations (34), (39) and (47)-(50) is by first finding the characteristic function (Fourier transform) of each component involved:

$$F_i(a) = \int_{\infty}^{\infty} p_i(w) \; \exp(jaw)\, dw, \qquad i = 1,2,\ldots,N \tag{51}$$

The overal PDF is then found by taking the inverse Fourier transform

$$p_W(w) = \frac{1}{2\pi} \int_{\infty}^{\infty} \{ \prod_{i=1}^{N} F_i(a) \; \exp(-jwa) \}\, da \tag{52}$$

In general, however, the integrations in equations (51) and (52) are rather difficult to evaluate analytically since only a limited number of functions have their Fourier transforms readily available. In addition, $p_i(w)$, $i=1,2,\ldots,N$, are generally stored in numerical form.

In practice, where the PDFs of the real and imaginary parts of

harmonic currents cannot be approximated by analytical functions, the Fourier transform method is not of practical value. Even if the Fourier transform of each PDF could be defined analytically, the total PDF would be very difficult (if not impossible) to obtain from the resultant Fourier transform. This is particularly true when a number of non-identical loads are involved.

There are two practical computation methods to evaluate the PDFs of the random harmonic currents and voltages: 1) direct integration using convolution and 2) Monte Carlo simulation, both of which are performed by computer. Each method has inherent advantages and disadvantages. In the first method, a number of different numerical algorithms are available to compute the convolution integral for determining the resultant distribution [62]-[63]. This method requires relatively less computation time, but may introduce large integration errors due to the eratic (not smooth) PDFs of the random harmonic currents. Figure 8 shows a flowchart of the numerical integration method.

The Monte Carlo simulation method utilizes repeated trials, the collection of which can be used to estimate the probability distribution. This method has recently been applied to a variety of complex power system problems [64]-[65]. However, one problem with the Monte Carlo simulation is the relatively large computation time and memory required to obtain results with satisfactory accuracy. Figure 9 illustrates in flowchart form the Monte Carlo method for determining the resultant PDFs of harmonic current injection and propagation.

4.5 Example and Discussion of Results

Let an analysis be desired of the 5-th order harmonic currents and

voltages of a hypothetical 3-bus distribution system shown in Fig. 10(a), where all impedance values are in per-unit values. The equivalent circuit for the 5-th harmonic is shown in Fig. 10(b) where the resistances and inductances are assumed to be frequency-independent.

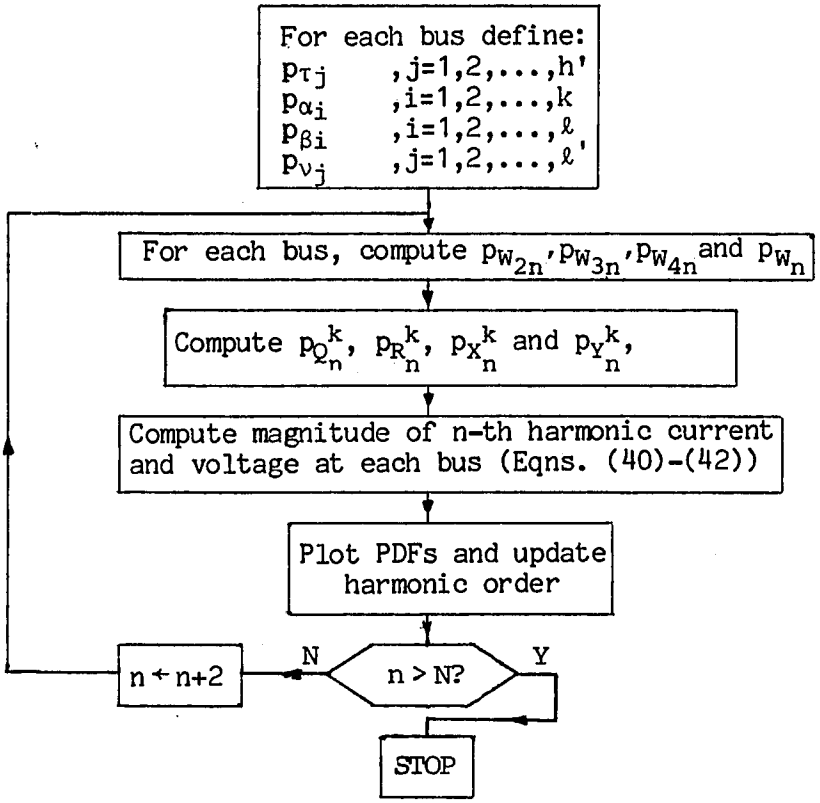

Fig. 8. Flowchart of Integration Method.

Since little relevant data on load and harmonic probability characteristics could be found in the literature, an arbitrary choice of different load characteristics was made. The nonlinear loads at bus 3 form a combination of all categories defined earlier but, for simplicity, it is assumed that all NLs of each category are identical. The following statistical data of the nonlinear loads may not be typically

realistic, but will illustrate the general technique that was developed and which is the primary purpose of this study.

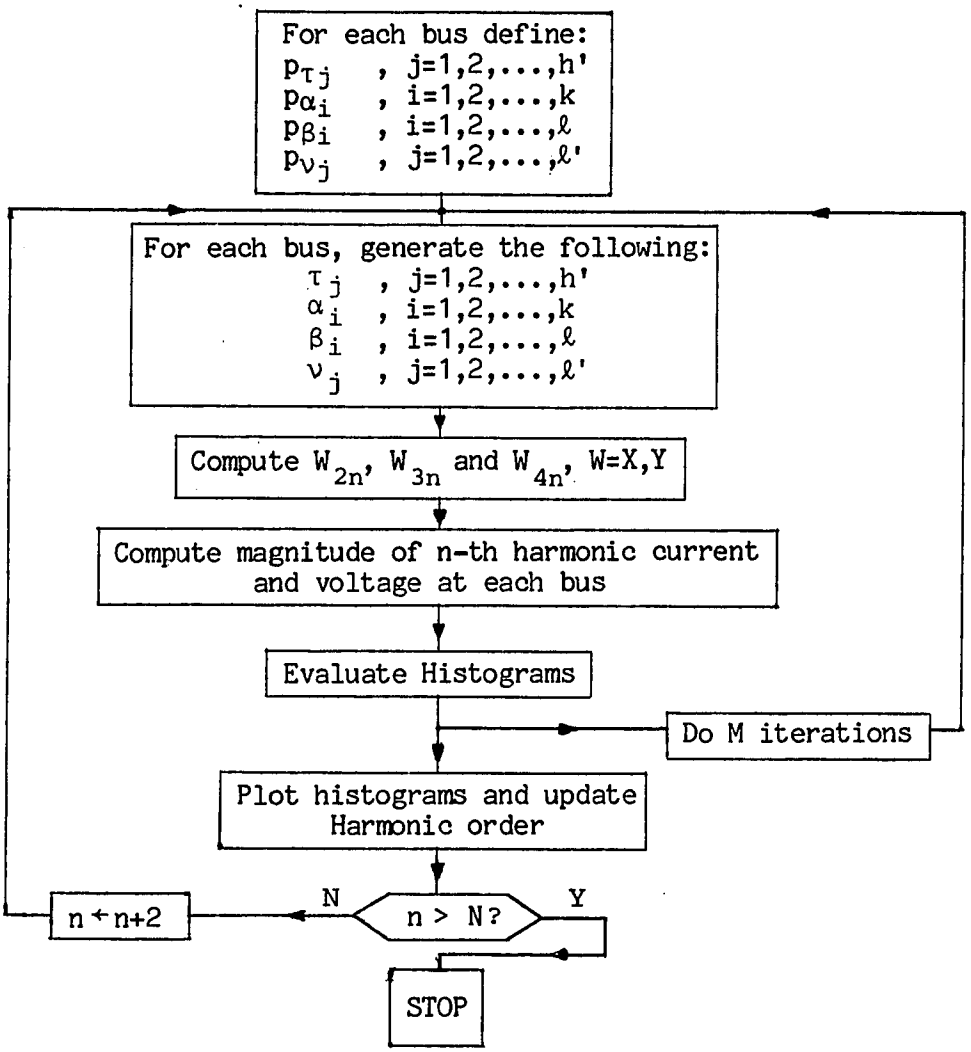

Fig. 9. Flowchart of Monte Carlo Simulation Method.

4.5.1 Statistical Data of Nonlinear Loads

1. **DNDC category** - Three ac/dc converters are switched ON from 7am to 5pm, each generating a steady 5-th harmonic current I_5 = 5A with zero phase angle (referred to the positive zero crossing of the fundamental voltage). In addition, an electric vehicle battery charger is turned ON

at midnight, then replaced by another every 8 hours. A typical battery charger generates a 5-th harmonic current whose magnitude and phase angle vary during the recharge cycle as shown in Fig. 11 [17].

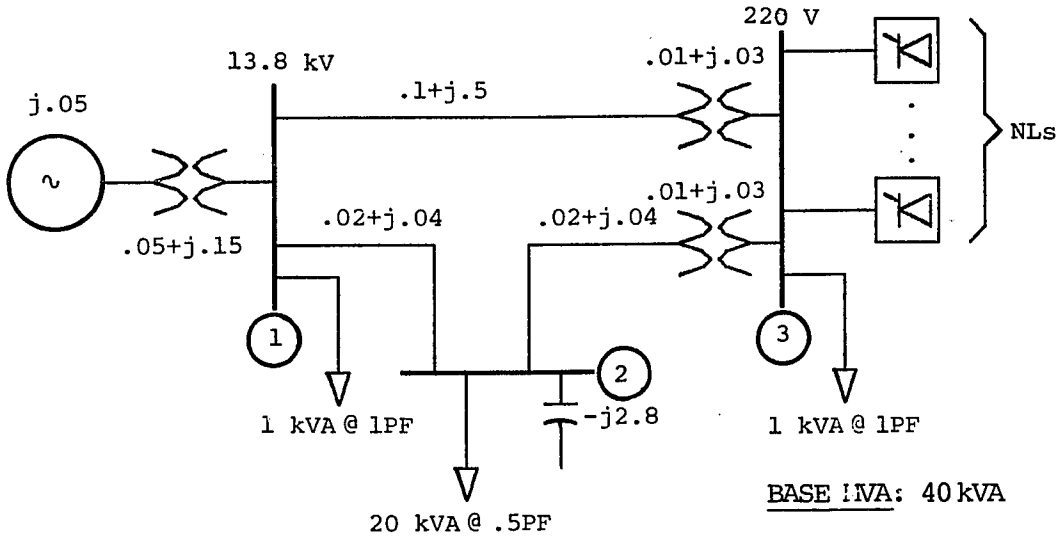

(a)

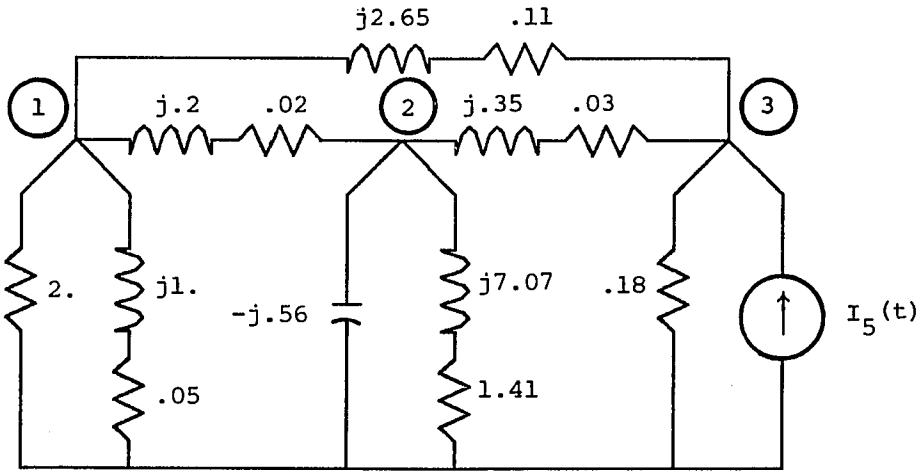

(b)

Fig. 10. Three-Bus Distribution System: (a) One-Line Diagram, (b) Equivalent Circuit for 5-th Harmonic.

2. **RNCC category** - There are 50 fluorescent lamps each generating a 5-th harmonic current of .07% of the fundamental ($\simeq$ 0.12A for a 240V/400W lamp), with zero phase angle [66]. The probability density function of

the number of lamps switched ON is binomial,

$$p_{T_i} = \binom{50}{i} p^i (1-p)^{50-i}, \qquad i=1,2,\ldots,50, \tag{53}$$

where p = .85 during business hours (7am - 5pm), and p = .25 for the rest of the day.

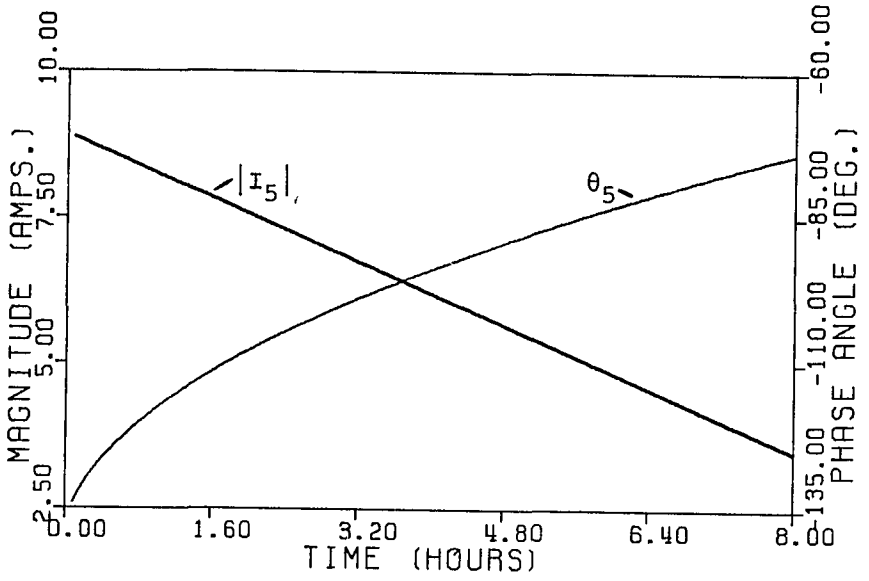

Fig. 11. 5-th Harmonic Current Generated Typical Battery Charger.

3. **CNRC category** - Between 7am and 5pm, 25 phase-controlled resistive loads are in service, each operating at 240V/400W, with a firing angle varying randomly and uniformly between 55° and 70°. The real and imaginary parts of the 5-th harmonic current generated by this type of load are respectively given by

$$X_5 = 5\{2\sin(6\alpha) - 3\sin(4\alpha)\}/36\pi \text{ A}$$

and

$$Y_5 = 5\{2\cos(6\alpha) - 3\cos(4\alpha)\}/36\pi \text{ A}.$$

4. **RNRC category** - In addition to the 25 phase-controlled resistive loads above, there are 10 more units of this load, but this number

varies randomly with a uniform distribution (p_{ν_j} = 0.1, j=1,2,...10) from noon to midnight. Otherwise, the firing angle β varies in the same fashion as α.

4.5.2 Simulation Results and Discussion

From the statistical data given above, it is seen that the 24-hr period can be composed of four time intervals. Each interval has the following combination of nonlinear load categories:

1. [12pm, 7am] - {DNDC, RNCC}
2. [7am, 12am] - {DNDC, RNCC, CNRC}
3. [12am, 5pm] - {DNDC, RNCC, CNRC, RNRC}
4. [5pm, 12pm] - {DNDC, RNCC, RNRC}

For each time interval, the probability density functions of the real and imaginary parts of the 5-th harmonic current injection were computed by numerical integration of equations (39), and were verified by the Monte Carlo simulation. Figure 12 shows these distributions for the 2nd, 3rd and 4th time intervals. In the first time interval, the random component of the imaginary part is zero but that of the real part is discrete in nature and is described by equation (53).

Note that all the distributions approach a normal density function (shown in dots) except for the imaginary part in the 4-th time interval. This component is generated only by the RNRC load category for which the central limit theorem cannot be applied since the number of loads changes randomly. Fig. 13 shows the distributions of the random component of the 5-th harmonic current magnitude computed by using equations (40)-(42). The dots show the results obtained by the Monte Carlo method.

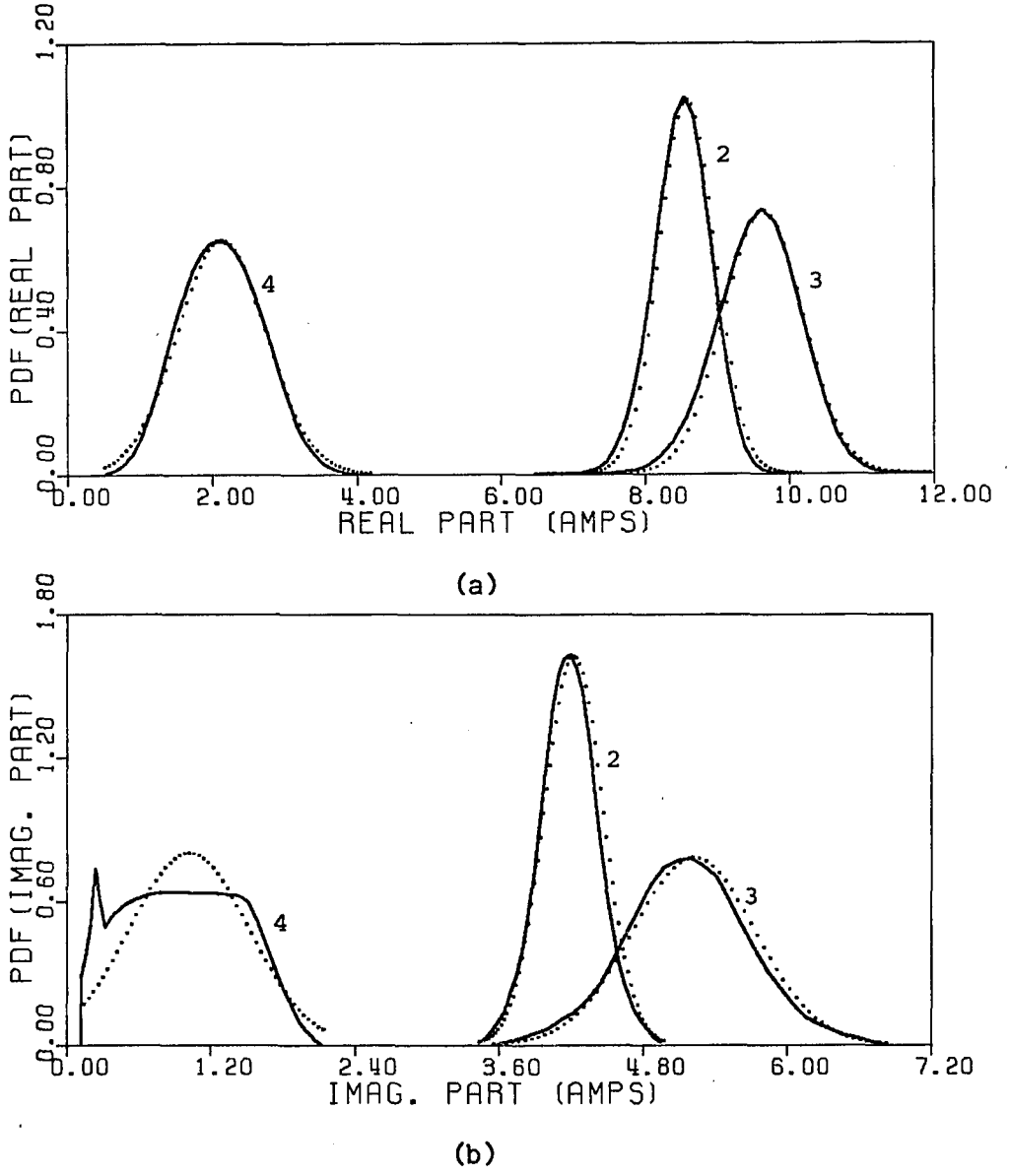

Fig. 12. PDFs of (a) Real and (b) Imaginary Parts of 5-th Harmonic Current in Time Intervals 2, 3 and 4.

A parameter of interest in the analysis of random harmonic currents is the expected value. The expected values of the x-y projections for the 5-th harmonic current were computed for each time interval and

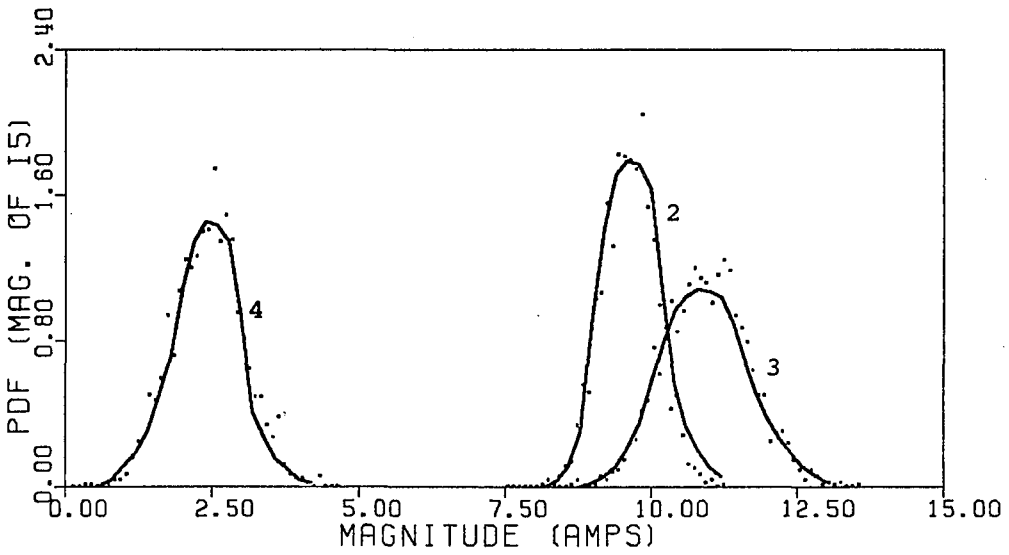

Fig. 13. PDFs of Random Component of 5-th Harmonic Current Magnitude in Time Intervals 2, 3 and 4.

the results were phasorially added with the deterministic components (currents generated by the ac-dc converters and battery chargers). Figure 14 shows the resultant harmonic current injection using the expected values of the random parts. The sudden changes at 7am and 5pm are obviously due to the switching of rectifier loads in the DNDC category. If the largest magnitudes of the 5-th harmonic currents generated by each nonlinear load are added arithmetically, a current of about 55 A is found. This "worst case" value exceeds by far (at times by a factor of 8) the expected current in Fig. 14.

From the above results, the PDFs of the x-y projections for the random components of the 5-th harmonic voltages and current propagations can be computed by equations (47)-(50) after converting the injected current in per-unit values. Then, equations (40)-(42) can be applied to compute the PDFs of the harmonic voltage magnitudes. Fig. 15 shows the

PDF of the random component of the 5-th harmonic voltage magnitude at bus 3 (verified by the Monte Carlo method in dots). Other information, such as expected values, maximum and minimum harmonic voltages and currents, could also be obtained from the above results.

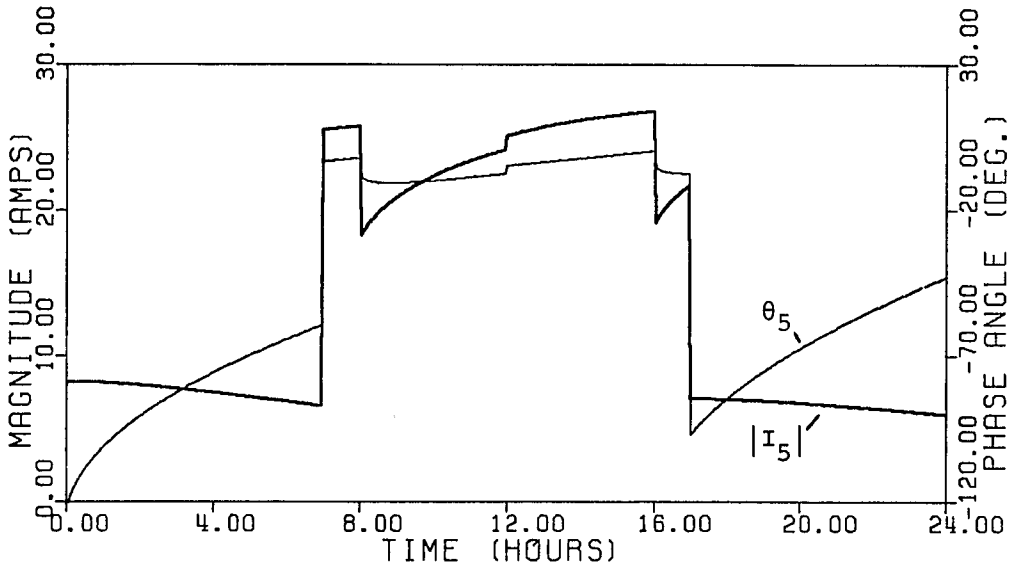

Fig. 14. Expected Value of 5-th Harmonic Current Versus Time.

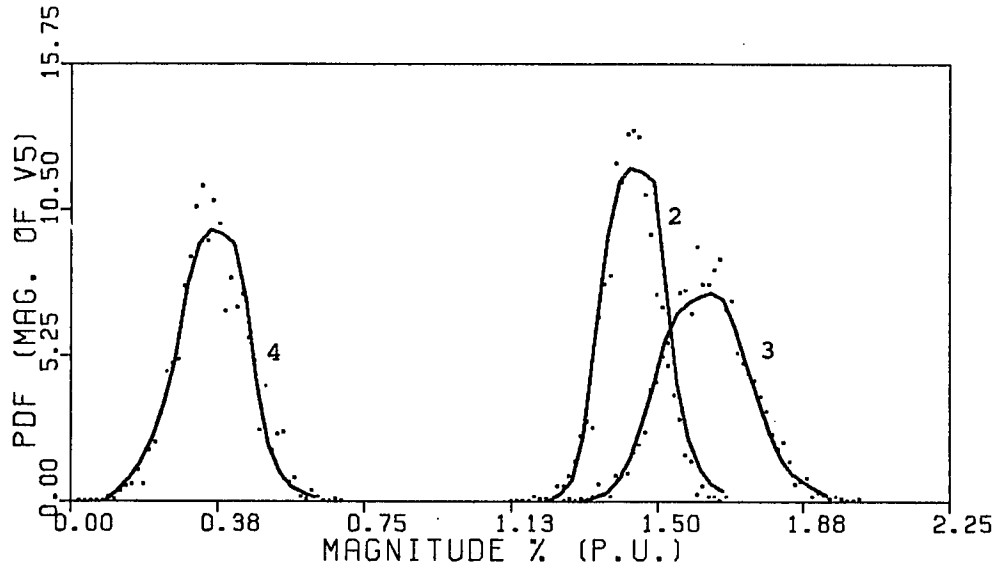

Fig. 15. PDFs of Random Component of 5-th Harmonic Voltage Magnitude at Bus 3 in Time Intervals 2, 3 and 4

4.6 Potential Applications

Accurate prediction of power system harmonic behavior will provide important information to utility companies and equipment designers. A few of the potential uses of the probabilistic model of harmonic current injection and propagation are described below.

4.6.1 Setting Limitations on Harmonic Levels

In the future, harmonic levels are expected to increase to intolerable levels. Several industrialized countries have already established some standards [67]-[68], but there is no uniform specification on the maximum permissible amount of wave distortion for current and voltage. Furthermore, existing regulations generally do not reflect harmonic variations and their randomness in power systems, and it is increasingly being recognized that more complete and accurate recommendations on allowable harmonic levels are needed.

For example, reference [27] sets a limit of 5% total voltage distortion for general industrial power systems at 2.4 to 69 kV. A relevant question is, "what if the probability of the distortion factor exceeding this limit is only 1% at all times?" This simple example clearly shows the importance of considering harmonic variations in setting maximum allowable harmonic levels.

The setting of harmonic standards should primarily take into account the effect of harmonics on equipment which can be classified in long-term and short-term effects. Long-term effects include thermal stress (copper, iron and dielectric losses) due to harmonics and related loss of equipment life. As an example, the IEEE Standard C57.12.00-1980, "General Requirement for Liquid-Immersed Distribution, Power and Regula-

ting Transformers", proposes a limit of a 5% distortion factor of the transformer load current. If the transformer load current has randomly varying harmonic components (e.g., caused by an arc furnace), then a certain chance or risk should be associated with the above limitations. Whenever the risk is higher than acceptable, harmonic filters should be recommended in order to conform to standards.

Short-term effects include insulation stress that is dependent on the instantaneous voltage magnitude. The maximum voltage magnitude in nonsinusoidal operating conditions may cause capacitor dielectric breakdown even for short time durations, particularly at resonance conditions. The probability characteristics of the maximum instantaneous voltage would be rather difficult to obtain since it also requires a knowledge of the phase angle of each harmonic voltage. However, given the PDFs of the x-y projections of each harmonic voltage, one could always resort to numerical evaluations to determine the probability that the total instantaneous voltage exceeds a prescribed limit at a given maximum risk.

4.6.2 Power Factor Correction

If a linear load is supplied by a nonsinusoidal voltage source with negligible internal impedance, it was found that the optimal power factor correction capacitor is [38]

$$C = \left[\sum_{n=1}^{N} n|V_n|B_n \right] / \left[\omega \sum_{n=1}^{N} (n|V_n|)^2 \right], \qquad (54)$$

where ω is the rated angular frequency and B_n is the load susceptance evaluated at the n-th harmonic frequency. The resulting optimal power factor is always less than unity since the distortion volt-amperes

cannot be compensated for by linear passive elements [38].

If the harmonic voltages vary randomly with known distributions, the capacitance as found by equation (54) will overcompensate the load at some time, and undercompensate it at other times. For such a case, it is suggested to select a capacitor value that corresponds to the expected value of the expression given in equation (54).

4.6.3 Communication Interference

Power system harmonics are known to generate telephone interference through inductive coupling. Telephone interference is measured by the Telephone Influence Factor (TIF) defined by equation (12). If the PDF of the rms of each harmonic voltage is known in a time interval, the distribution of the TIF can be found by certain elaborate computations. From the resulting characteristics, one can deduce the probability of exceeding the TIF limitations at any time of the day.

4.6.4 Estimating Line Losses

Since harmonic currents are changing with time, so are their rms values. Therefore, the energy loss in transmission lines varies accordingly. The expected power loss in a line at any instant can be computed from equation (6) after replacing I_n^2, n=1,...,N by their mean values.

The probabilistic harmonic model may also be used to compute the expected maximum heating (maximum rms current squared) and insulation stress (maximum instantaneous voltage) of a long transmission line based on the techniques presented in Refs. [20]-[69].

4.6.5 Equipment Design

Harmonic filtering is one of the primary methods of harmonic reduction for large converter installations. These filters are designed to reduce harmonic current levels and provide all, or part of, the reactive power consumed by the converter. Furthermore, the filter size depends on both the magnitude of the harmonic current it absorbes and the VARs its generates. Thus the knowledge of the changes in harmonic current levels can help in the design of more effective and economical harmonic filters. The information provided by the probability characteristics of power system harmonics can also reduce the cost of measures taken to prevent equipment (e.g., transformers and rotating machines) from excessive heating caused by harmonics.

5. MAXIMUM HEATING AND INSULATION STRESS ON UNTRANSPOSED TRANSMISSION LINES UNDER NONSINUSOIDAL CONDITIONS

Harmonic levels in power systems can be accurately predicted by several computer methods which were discussed in chapter 3, namely, the nonlinear time domain simulation [50], the linearized model or current injection technique [13] and the nonlinear frequency domain analysis [14]. While these methods give accurate results for the bus voltage and current harmonics, information concerning the maximum values of the overall rms current and peak voltage on long transmission lines are not readily available since the lines are represented by their π-equivalents. These maxima could be larger than the corresponding values at the line terminals and, if ignored, insulation damage, overheating or communication interference may occur.

One method to determine the magnitude and location of the global maxima of rms current and peak voltage is to represent the line by a sufficient number of nominal π-models connected in cascade. However, this approach has computational, storage and accuracy problems.

Shultz, Smith and Hickey [20] proposed a method to find the maximum rms current and peak voltage of a single harmonic on an equivalent single-phase transmission line. This method can be applied to obtain the maximum inductive interference at each harmonic frequency. It is recognized [20], however, that the maximum rms value of the total current and the maximum peak value of the instantaneous voltage are of greater importance since at the locations where they occur, maximum line heating and insulation stress, respectively, take place. Furthermore, transmission lines are generally untransposed because of the high cost of transpositions [21], and recent studies [70], [71] show that un-

balanced harmonic current injection is likely to be found in practical systems. Therefore, it is of interest to find these maxima in a more realistic condition.

In this chapter, an untransposed three-phase transmission line under unbalanced operating conditions is considered [72]. First, analytical expressions for a single current and voltage harmonic of an equivalent three-conductor line are briefly formulated through a modal transformation. Then, efficient numerical methods are presented for finding the global maxima of the total rms current and peak voltage if the computed or measured harmonics at one end of the transmission line are known. The first method for computing the maximum rms current is based on Shubert's algorithm [73], which converges directly to the global maximum (global convergence method). The second method employs the Golden Section search algorithm to compute the local maxima in some prescribed regions where the rms current represents a unimodal function (local convergence method). The numerical algorithm for evaluating the maximum peak voltage is also based on the local convergence method where the steepest ascent approach is used to calculate all the local maxima. Another application of the procedure considered is the determination of the maximum distortion factors of voltage and current. Finally, the special case of single-phase transmission lines is examined. The methods are illustrated by a numerical example.

5.1 Expression for Single Harmonic

The procedure to obtain the series impedance and shunt admittance matrices of an equivalent three-conductor line is well documented [21], [74]. For convenience, the basic equations and expressions for

the frequency-dependent elements of the impedance and admittance matrices are summarized in Appendix II. At a point x miles from the receiving end of the line, the voltage and current wave equations for the n-th harmonic frequency are given by

$$[d^2\bar{V}^n/dx^2] = [\bar{Z}^n][\bar{Y}^n][\bar{V}^n] \tag{55}$$

and

$$[d^2\bar{I}^n/dx^2] = [\bar{Y}^n][\bar{Z}^n][\bar{I}^n] \tag{56}$$

where $[\bar{V}^n]$ and $[\bar{I}^n]$ are column vectors representing the phase voltages and currents. The series impedance and shunt admittance matrices, $[\bar{Z}^n]$ and $[\bar{Y}^n]$, include the effects of unbalanced configuration, and the use of bundled conductors and ground wires.

On a multiphase transmission line, the mutual elements of the series impedance and shunt admittance matrices allow the traveling waves to couple across the phases. The simultaneous equations describing the propagation on each phase are therefore interdependent.

Since $[\bar{Z}^n]$ and $[\bar{Y}^n]$ matrices are derived for unsymmetrical lines, transformation into symmetrical components will not diagonalize these matrices. Consequently, a current flow of one sequence will give rise to voltages of all sequences (i.e., the sequence networks are mutually coupled). Thus, it is clear that asymmetry cannot be studied conveniently by using the symmetrical component reference frame. Instead, a modal transformation will be used to diagonalize the matrices.

It is possible to transform (55) and (56) into decoupled equations by tranforming phase voltages and currents into their modal form:

$$[\bar{V}^n] = [\bar{T}^n][\bar{V}'^n]$$

and

$$[\bar{I}^n] = [\bar{M}^n][\bar{I}'^n]$$

where the transformation matrices $[\bar{T}^n]$ and $[\bar{M}^n]$ are respectively composed of the eigenvectors of the products $[\bar{Z}^n][\bar{Y}^n]$ and $[\bar{Y}^n][\bar{Z}^n]$. Equations (55) and (56) can be converterd into

$$[d^2V'^n/dx^2] = [\bar{\gamma}^{2n}][V'^n]$$

and

$$[d^2V'^n/dx^2] = [\bar{\gamma}^{2n}][I'^n]$$

where $[\bar{\gamma}^{2n}]$ is a diagonal matrix whose elements are the eigenvalues of the matrix product $[\bar{Z}^n][\bar{Y}^n]$ (the matrix product $[\bar{Y}^n][\bar{Z}^n]$ has the same eigenvalues as $[\bar{Z}^n][\bar{Y}^n]$).

Once the modal voltages and currents are solved in terms of receiving end voltages $[\bar{V}_r^n]$ and currents $[\bar{I}_r^n]$, the solution is transformed back into phase quantities. The resulting solutions to (55) and (56) are respectively given by [75]

$$[\bar{V}^n(x)] = [\bar{S}^n] \quad [\cosh(\bar{\gamma}_k^n x)][\bar{P}^n] + [\bar{\gamma}_k^n \sinh(\bar{\gamma}^n x)][\bar{Q}^n] \tag{57}$$

and

$$[\bar{I}^n(x)] = [\bar{M}^n] \quad [\frac{1}{\bar{\gamma}_k^n}\sinh(\bar{\gamma}_k^n x)][\bar{P}^n] + [\cosh(\bar{\gamma}_k^n x)][\bar{Q}^n] \tag{58}$$

where

$$[\frac{1}{\bar{\gamma}_k^n}\sinh(\bar{\gamma}_k^n x)] = \mathrm{diag}\{\frac{1}{\bar{\gamma}_a^n}\sinh(\bar{\gamma}_a^n x), \frac{1}{\bar{\gamma}_b^n}\sinh(\bar{\gamma}_b^n x), \frac{1}{\bar{\gamma}_c^n}\sinh(\bar{\gamma}_c^n x)\}$$

$$[\bar{\gamma}_k^n \sinh(\bar{\gamma}_k^n x)] = \mathrm{diag}\{\bar{\gamma}_a^n \mathrm{sing}(\bar{\gamma}_a^n x), \bar{\gamma}_b^n \sinh(\bar{\gamma}_b^n x), \bar{\gamma}_c^n \sinh(\bar{\gamma}_c^n x)$$

$$[\cosh(\bar{\gamma}_k^n x)] = \mathrm{diag}\{\cosh(\bar{\gamma}_a^n x), \cosh(\bar{\gamma}_b^n x), \cosh(\bar{\gamma}_c^n x)\}$$

$$\bar{\gamma}_k^n = \alpha_k^n + j\beta_k^n, \quad k=a,b,c,$$

$$[\bar{P}^n] = [\bar{M}^n]^{-1}[\bar{Y}^n][\bar{V}_r^n],$$

$$[\bar{Q}^n] = [\bar{M}^n]^{-1}[\bar{I}_r^n],$$

$$[\bar{S}^n] = [\bar{Y}^n]^{-1}[\bar{M}^n].$$

Under perfectly balanced and symmetrical conditions, the modal transformation matrices $[\bar{T}^n]$ and $[\bar{M}^n]$ become both identical to the symmetrical component transformation matrix:

$$[\bar{T}^n] = [\bar{M}^n] = \begin{bmatrix} 1 & 1 & 1 \\ 1 & \bar{a}^2 & \bar{a} \\ 1 & \bar{a} & \bar{a}^2 \end{bmatrix}, \quad \bar{a} = \exp(j2\pi/3).$$

Therefore, the modal networks become sequence networks. Furthermore, it is well known that in a balanced system, the individual harmonic components of voltages and currents are entirely zero sequence (3q), positive sequence (3q+1), or negative sequence (3q-1), where q is an integer.

Transformation of equations (55) and (56) result in scalar differential equations of some sequence component that depends on the harmonic order. Then, the resulting equations (in phase quantities) are the same as those of a single-phase transmission line which is treated in section 5.5.

5.2 Maximum Single Harmonic Current and Voltage

To simplify the notation, let phases a, b and c be represented by subscripts 1, 2 and 3 respectively. From Eqn. (58), the n-th harmonic current of phase k (=1,2,3) can be written as

$$\bar{I}_k^n(x) = \sum_{i=1}^{3} \{I_{ki}^{n\pm} \exp(\bar{\gamma}_i^n x) + I_{ki}^{n\pm} \exp(-\bar{\gamma}_i^n x)\} \qquad (59)$$

where

$$I^{n\pm} = \frac{1}{2\bar{\gamma}_i^n} \bar{M}_{ki}^n \ (\bar{\gamma}_i^n \bar{Q}_i^n \pm \bar{P}_i^n) = I_{ki}^{n\pm} \angle \theta_{ki}^{n\pm}.$$

The current in (59) can be expressed in terms of its real and imaginary parts:

$$\begin{bmatrix} Re\{\bar{I}_k^n(x)\} \\ Im\{\bar{I}_k^n(x)\} \end{bmatrix} = \sum_{i=1}^{3} \begin{bmatrix} \cos(\beta_i^n x+\theta_{ki}^{n+}) & \cos(-\beta_i^n x+\theta_{ki}^{n-}) \\ \sin(\beta_i^n x+\theta_{ki}^{n+}) & \sin(-\beta_i^n x+\theta_{ki}^{n-}) \end{bmatrix} \begin{bmatrix} I_{ki}^{n+}\exp(\alpha_i^n x) \\ I_{ki}^{n-}\exp(-\alpha_i^n x) \end{bmatrix}. \quad (60)$$

Since the rms value squared of the n-th harmonic current of phase k is the sum of the squares of its real and imaginary parts, from (60) follows

$$I_k^{n\,2}(x) = \sum_{i=1}^{3} \{A_i^n + 2 \sum_{\substack{j=1 \\ \neq i}} B_{ij}^n\} + 2 \sum_{i=1}^{2} \sum_{j=i+1}^{3} \{C_{ij}^n + D_{ij}^n\} \quad (61)$$

where

$$A_i^n = \{I_{ki}^{n+}\exp(\alpha_i^n x)\}^2 + \{I_{ki}^{n-}\exp(-\alpha_i^n x)\}^2 + 2I_{ki}^{n+}I_{ki}^{n-}\cos(2\beta_i^n x+\theta_{ki}^{n+}-\theta_{ki}^{n-}),$$

$$B_{ij}^n = I_{ki}^{n+}I_{kj}^{n-}\exp\{(\alpha_i^n-\alpha_j^n)x\}\cos\{(\beta_i^n+\beta_j^n)x+\theta_{ki}^{n+}-\theta_{kj}^{n-}\},$$

$$C_{ij}^n = I_{ki}^{n+}I_{kj}^{n+}\exp\{(\alpha_i^n-\alpha_j^n)x\}\cos\{(\beta_i^n-\beta_j^n)x+\theta_{ki}^{n+}-\theta_{kj}^{n+}\},$$

and

$$D_{ij}^n = I_{ki}^{n-}I_{kj}^{n-}\exp\{-(\alpha_i^n+\alpha_j^n)x\}\cos\{(\beta_j^n-\beta_i^n)x+\theta_{ki}^{n-}-\theta_{kj}^{n-}\}.$$

It is apparent that a numerical evaluation is required to find the global maximum of $I_k^{n2}(x)$. In the following, two sequential search algorithms which guarantee locating the global maximum of the objective function $I_k^{n2}(x)$ will be formulated. The first method applies Shubert's algorithm [73] which converges to the global maximum. The second method computes all the local maxima by applying the Golden Section search in specific intervals on the transmission line.

5.2.1 Global Convergence Method

The only requirement needed for the application of Shubert's algorithm is that the objective function be globally Lipschitzian (i.e., some bound on its rate of change for the entire line length must be

available). Thus, the Lipschitz constant L_k^n, as defined by

$$|I_k^{n2}(x_2) - I_k^{n2}(x_1)| = L_k^n|x_2 - x_1|$$

for all x_1, x_2 less than ℓ, must be finite and known.

For a differentiable objective function such as $I_k^{n2}(x)$ in (61), this amounts to finding some upper bound on its derivative. Since the propagation constants α_i^n, i=1,2,3, are relatively small for any harmonic frequency of interest, L_k^n may be approximated by

$$L_k^n = \sum_{i=1}^{3} \{4\beta_i^n I_{ki}^{n+} I_{ki}^{n-} + 2 \sum_{\substack{j=1 \\ \neq i}} I_{ki}^{n+} I_{kj}^{n-} (\beta_i^n + \beta_j^n)\} + \sum_{i=1}^{2} \sum_{j=i+1}^{3} |\beta_i^n - \beta_j^n| (I_{ki}^{n+} I_{kj}^{n+} + I_{ki}^{n-} I_{kj}^{n-}) \tag{62}$$

The algorithm is based on selecting some initial point x_1 inside the interval $[0, \ell]$, and generating a recursive sampling sequence as follows. Let

$$F(x) = \min_{m=1,2,\ldots,h} \{I_k^{n2}(x_m) + L_k^n|x - x_m|\} \tag{63}$$

and

$$M_h = \max_{x\in[0,\ell]} F_h(x), \tag{64}$$

then choose x_{h+1} such that

$$F_h(x_{h+1}) = M_h. \tag{65}$$

The above sequential method is proven to converge effectively to the global maximum [73]. In the computation process, the function $F_h(x)$ defined in Eqn. (63) is conveniently stored in an ordered set

$$D_m = \{(x_{11}, y_{11}), \ldots, (x_{im}, y_{im})\}, \qquad y_{11} \leq \ldots \leq y_{im},$$

where the vectors (x_{im}, y_{im}) are coordinates of the maxima of $F_h(x)$. The initial set of data depends, of course, on the choice of thefirstsampling point x_1. Figure 16 shows the flowchart of the global convergence method when x_1 is chosen at the center of the line.

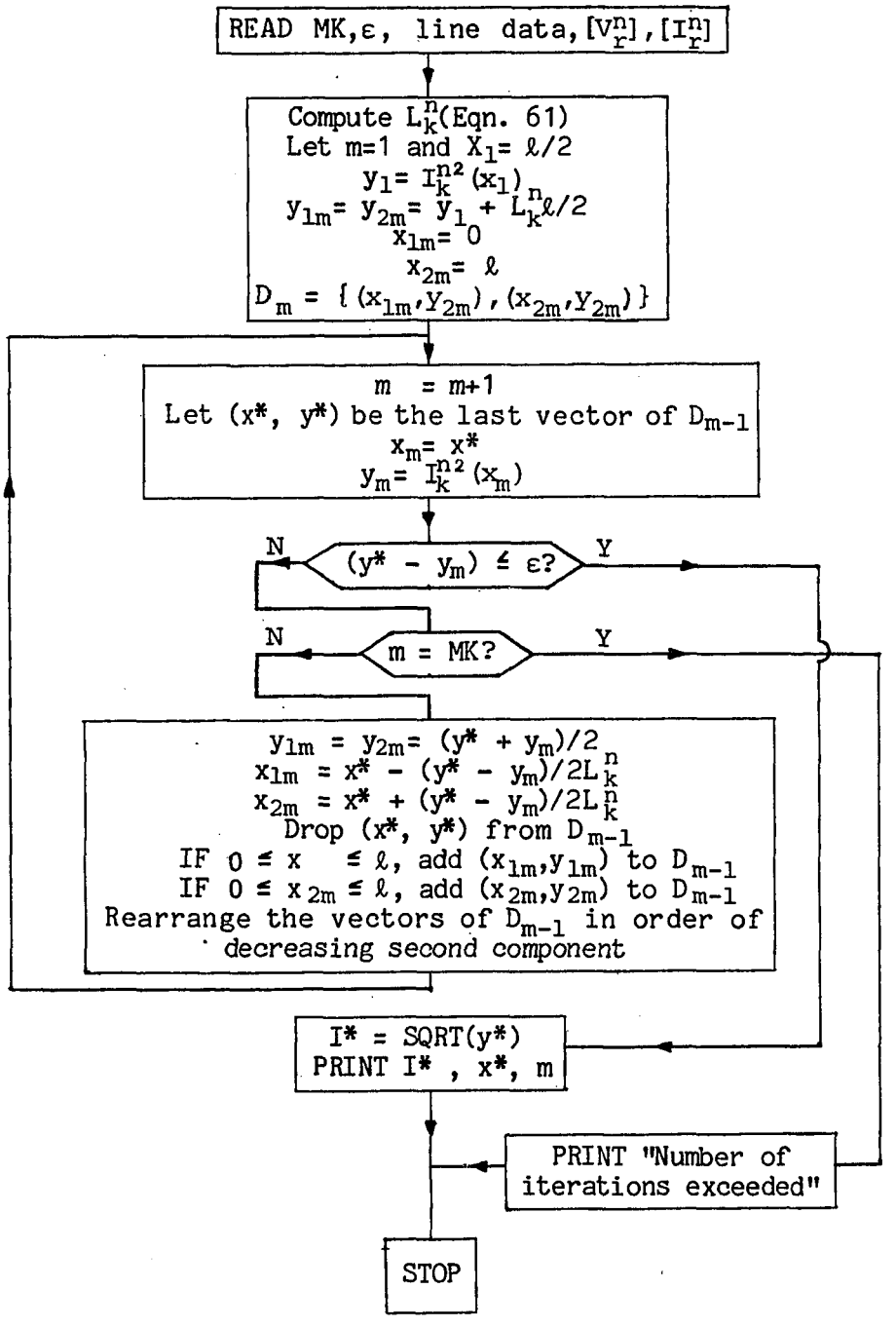

Fig. 16. Flowchart of Global Convergence Method.

5.2.2 Local Convergence Method

Since the objective function $I_k^{n2}(x)$ generally has a number of local

maxima for a given line length, existing direct search methods will successfully reach one local maximum which in itself is of little practical value. To find all the local maxima, the line is divided into regions within each of which the objective function is unimodal. By determining and comparing the local maxima of these regions, the global maximum can be readily identified.

An examination of equation (61) indicates that $I_k^{n2}(x)$ is a sum of exponential functions and exponential-cosine functions. Each of these functions is either convex or concave and strictly increasing or decreasing in specific intervals whose boundaries are defined by

$$x = \frac{2\theta_k^n + m\pi}{2\beta_k^n}, \qquad m = 0,1,2,\ldots , \tag{66}$$

where β_k^n and θ_k^n respectively represent the coefficients of x in the cosine terms and the corresponding angles at the receiving end. These locations along with the line boundaries are next arranged in increasing order: $x_1(=0) < x_2 < \ldots < x_k(=\ell)$. Then, in any interval $[x_i, x_{i+1}]$, on the transmission line, each term of (61) is a strictly concave or convex function. Consequently, $I_k^{n2}(x)$ is a summation of strictly convex and concave functions in $[x_i, x_{i+1}]$. Considering that the sum of strictly convex (concave) functions is also a strictly convex (concave) function [76], and the sum of a strictly convex and concave function is unimodal, $I_k^{n2}(x)$ is a unimodal function in each interval. Therefore, application of a direct search method guarantees convergence in each interval.

Since the global maximum of the total rms current is of interest in this study, it is suggested that the derivative of $I_k^{n2}(x)$ be evaluated

at x_1, x_2 ..., x_j. If this derivative changes sign from plus at x_i, i=1,2...,k-1, to minus at x_{i+1}, then there exists a local maximum in $[x_i, x_{i+1}]$, and its value can be found by any of the one-dimensional search techniques.

Because of its effectiveness, the Golden Section search was selected for computing the local maxima. Once all the local maxima are identified, the global maximum is simply the largest of them. The algorithm of this method is summarized by the flowchart shown in Fig. 17.

5.3 Maximum Overall RMS Current and Peak Voltage

The total rms current squared of phase k is defined by

$$I_k^2(x) = \sum_{n=1}^{N} I_k^{n2}(x) \tag{67}$$

where $I_k^{n2}(x)$ is given in (61) and N is the highest harmonic order of interest. The same computational methods of the previous section can be readily used to determine the global maximum of (67). The Lipschitz constant required by the global convergence method is

$$L_k = \sum_{n=1}^{N} L_k^n \, . \tag{68}$$

When applying the local convergence method, the set of points defining the intervals where $I_k^2(x)$ satisfies the unimodality condition is given by Eqn. (66) where n=1,...,N. The line intervals are then defined by arranging these solutions in increasing order.

The n-th harmonic voltage of phase k can be rewritten similar to the current equation in (59):

$$\bar{V}_k^n(x) = \sum_{i=1}^{3} \{\bar{V}_{ki}^{n+} \exp(\bar{\gamma}_i^n x) + \bar{V}_{ki}^{n-} \exp(-\bar{\gamma}_i^n x)\}$$

$$= \sum_{i=1}^{3} V_{ki}^{n}(x) \angle\psi_{ki}^{n}(x) \qquad (69)$$

where

$$\bar{V}_{ki}^{n\pm} = \frac{1}{2} \bar{S}_{ki}^{n} (\bar{P}_i^n \pm \bar{\gamma}_i^n \bar{Q}_i^n) = V_{ki}^{n\pm} \angle\delta_{ki}^{n\pm}.$$

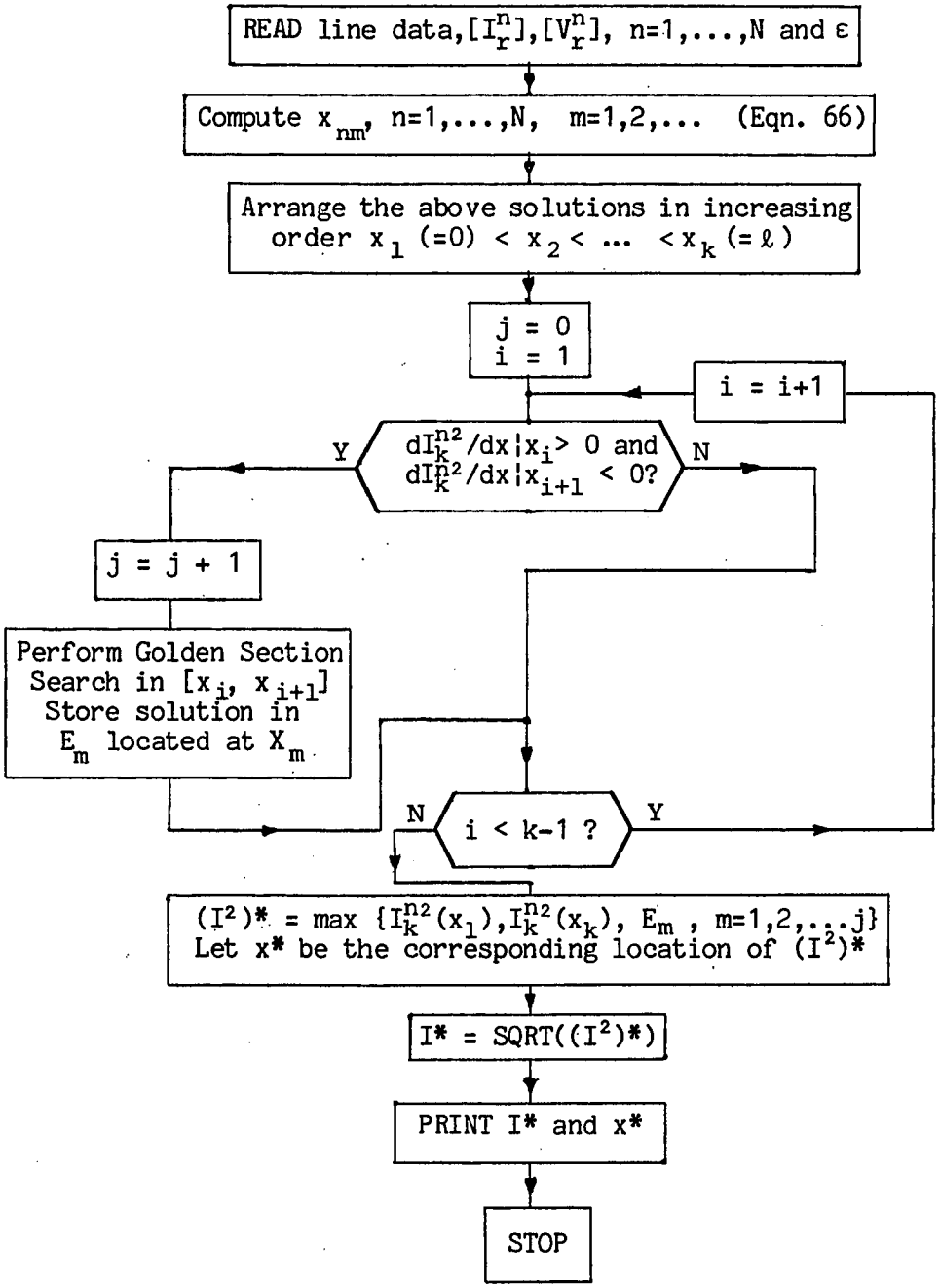

Fig. 17. Flowchart of Local Convergence Method.

The overall instantaneous voltage is then given by

$$V_k(x,t) = \sqrt{2} \sum_{n=1}^{N} \sum_{i=1}^{3} V_{ki}^n(x) \sin(n\omega_o t - \psi_{ki}^n(x))$$

$$= \sqrt{2} \sum_{n=1}^{N} \sum_{i=1}^{3} [Re\{\bar{V}_{ki}^n(x)\} \sin(n\omega_o t) - Im\{\bar{V}_{ki}^n(x)\}\cos(n\omega_o t)] \quad (70)$$

where the real and imaginary parts of $\bar{V}_{ki}^n$ are found from (60) after substituting $(I_{ki}^{n\pm}, \theta_{ki}^{n\pm})$ by $(V_{ki}^{n\pm}, \delta_{ki}^{n\pm})$.

The point of maximum insulation stress, i.e., the line location where $v_k(x,t)$ is maximum could be found by setting the partial derivatives of (69) with respect to x and t equal to zero. However, no closed form solution exists for the resulting equations. Hence, a numerical evaluation is required. Shubert's method does not seem to be computationally feasible for an objective function with more than one variable. Recursive numerical methods for optimizing a two-dimensional function are generally effective only if the function is confined to a region in which the function is locally unimodal. Therefore, the specific regions of the x-t plane, where $v_k(x,t)$ satisfies the unimodality, need to be identified.

Consider the i-th term of the n-th harmonic voltage $v_k(x,t)$. The peak voltage, $\sqrt{2}\, V_{ki}^n(x)$ varies with x according to the square root of the right hand side of (61) if $(V_{ki}^{n\pm}, \delta_{ki}^{n\pm})$ is substituted for $(I_{ki}^{n\pm}, \theta_{ki}^{n\pm})$. Since α_i^n is small for all harmonic orders of interest, the locations where the first and second derivatives of the peak value relative to distance are zero can be respectively approximated by

$$x_m = \frac{\delta_{ki}^{n-} - \delta_{ki}^{n+} + m\pi}{2\beta_i^n}, \qquad m = 0,1,\ldots, \quad (71)$$

and

$$x_m = \frac{\delta_{ki}^{n-} - \delta_{ki}^{n+} + \arccos(-u + \sqrt{u^2 - 1}) + 2\pi m}{2\,\beta_i^n}, \quad m = 0,1,\ldots, \qquad (72)$$

where

$$u = \frac{(V_{ki}^{n+})^2 + (V_{ki}^{n-})^2}{2\beta_i V_{ki}^{n+} V_{ki}^{n-}} .$$

For a given x_m, the time instants when $v_k(x_m,t)$ is maximum, zero or minimum are given by

$$t_{mj} = \frac{2\psi_{ki}^n(x) + j\pi}{2n\omega_o}, \quad j = 0,1,\ldots \quad . \qquad (73)$$

In general, the magnitudes of harmonic voltages at the transmission level are relatively small; thus, the overall peak voltage is expected to occur in the neighborhood of the peak of the fundamental component. A conservative estimate is that the global peak occurs within $\pm 45^o$ or $\pm 1/8f_o$ seconds from the instant when the fundamental peak occurs. Therefore, only those solutions of (73) that fall within this interval are selected.

The solutions (71) and (72) on the transmission line along with the corresponding time instants given by (73) are arranged in increasing order (x_m, t_{mj}), m=1,2,... j=1,2,... where $x_1 < x_2 < \ldots$ and $t_1 < t_2 < \ldots$. Then it is clear that $v_{ki}(x,t)$ is strictly convex or concave in the region defined by (x_m,t_{mj}), $(x_m,t_{m,j+1})$, $(x_{m+1},t_{m+1,j})$ and $(x_{m+1}, t_{m+1,j+1})$.

By applying the above procedure to all terms in (69), the line locations given by (71) and (72) are arranged in increasing order: $x_1(=0) < \ldots < x_k(=\ell)$. For each x_m, the time instants of (73) are also arranged in the same fashion: $t_1(=1/8f_o) < \ldots < t_j(=3/8f_o)$. Then, in

every region defined by (x_m, t_{mj}), $(x_m, t_{m,j+1})$, $(x_{m+1}, t_{m+1,j})$ and $(x_{m+1}, t_{m+1,j+1})$, the overall instantaneous voltage $v_k(x,t)$ is a unimodal function (by the same reasoning as that for the maximum rms current). The local maxima of $v_k(x,t)$ can then be found by any existing search method.

Because of the fact that only regions with local maxima need to be investigated, it is suggested that the gradient of $v_k(x,t)$ be evaluated. A necessary condition for a local maximum to exist in a region is that $\partial v_k(x,t)/\partial x$ be positive at both (x_m, t_{mj}) and $(x_m, t_{m,j+1})$, and negative at both $(x_{m+1}, t_{m+1,j})$ and $(x_{m+1}, t_{m+1,j+1})$. Upon satisfying this requirement, a further selection of the regions can be made by verifying the directions of the slope projections on the x-t plane. Only those regions with slope projections pointing toward the region interior have a local maxima:

$$\frac{\partial V/\partial t}{\partial V/\partial x}(x_{m+1}, t_{m+1,j}) \leq G_{mj} \leq \frac{\partial V/\partial t}{\partial V/\partial x}(x_m, t_{mj}) \tag{74}$$

$$\frac{\partial V/\partial t}{\partial V/\partial x}(x_m, t_{m,j+1}) \leq H_{mj} \leq \frac{\partial V/\partial t}{\partial V/\partial x}(x_{m+1}, t_{m+1,j+1}) \tag{75}$$

where

$$G_{mj} = (t_{m+1,j} - t_{mj})/(x_{m+1} - x_m)$$

and

$$H_{mj} = (t_{m+1,j+1} - t_{m+1,j})/(x_{m+1} - x_m) \ .$$

Thus only the regions satisfying the above conditions need to be analyzed. The initial point to start the search is selected to be the center of each of these regions:

$$\{x_o, t_o\} = \{\tfrac{1}{2}(x_m + x_{m+1}), \ \tfrac{1}{4}(t_{mj} + t_{m,j+1} + t_{m+1,j} + t_{m+1,j+1})\}. \tag{76}$$

The steepest ascent method is selected to evaluate the local maxima. This method requires the gradient of the objective function $v_k(x,t)$:

$$\nabla v_k(x,t) = \begin{bmatrix} \frac{\partial v}{\partial x} \\ \frac{\partial v}{\partial t} \end{bmatrix} = \sum_{n=1}^{N} \sum_{i=1}^{3} \begin{bmatrix} U'^{n}_{ki}(x)\sin(n\omega_o t) - W'^{n}_{ki}(x)\cos(n\omega_o t) \\ n\omega_o U^{n}_{ki}(x)\cos(n\omega_o t) + n\omega_o W^{n}_{ki}(x)\sin(n\omega_o t) \end{bmatrix} \quad (77)$$

where

$$\begin{bmatrix} U'^{n}_{ki}(x) \\ W'^{n}_{ki}(x) \end{bmatrix} = \gamma^{n}_{i} \begin{bmatrix} \cos(\zeta^{n}_{i}+\delta^{n+}_{ki}+\beta^{n}_{i}x) & -\cos(\zeta^{n}_{i}+\delta^{n-}_{ki}-\beta^{n}_{i}x) \\ \sin(\zeta^{n}_{i}+\delta^{n+}_{ki}+\beta^{n}_{i}x) & -\sin(\zeta^{n}_{i}+\delta^{n-}_{ki}-\beta^{n}_{i}x) \end{bmatrix} \begin{bmatrix} V^{n+}_{ki}\exp(\alpha^{n}_{i}x) \\ V^{n-}_{ki}\exp(-\alpha^{n}_{i}x) \end{bmatrix}$$

The flowchart in Fig. 18 summarizes the algorithm for computing the maximum peak voltage.

Since the line-to-neutral voltages are likely to be differently distributed along the line, the line-to-line voltages may have quite unexpected patterns. Therefore, it is also of interest to determine the maximum peak of the line voltage.

The n-th harmonic complex voltage between phases a and b is derived from (69):

$$\bar{V}_{ab}(x) = \sum_{i=1}^{3} \{\bar{V}^{n+}_{abi} \exp(\bar{\gamma}^{n}_{i}x) + \bar{V}^{n-}_{abi} \exp(-\bar{\gamma}^{n}_{i}x)\}$$

$$= \sum_{i=1}^{3} V^{n}_{abi}(x) \exp\{j\psi^{n}_{abi}(x)\} \quad (78)$$

where

$$\bar{V}^{n\pm}_{abi} = \bar{V}^{n\pm}_{ai} - \bar{V}^{n\pm}_{bi} .$$

The corresponding overall instantaneous voltage is

$$v_{ab}(x,t) = \sqrt{2} \sum_{n=1}^{N} \sum_{i=1}^{3} V^{n}_{abi}(x) \sin(n\omega_o t - \psi^{n}_{abi}(x)\}. \quad (79)$$

The algorithm used to compute the maximum peak phase-voltage can be readily used to determine the maximum peak line-voltage by using (71)-(73), however, applied to (78) and (79).

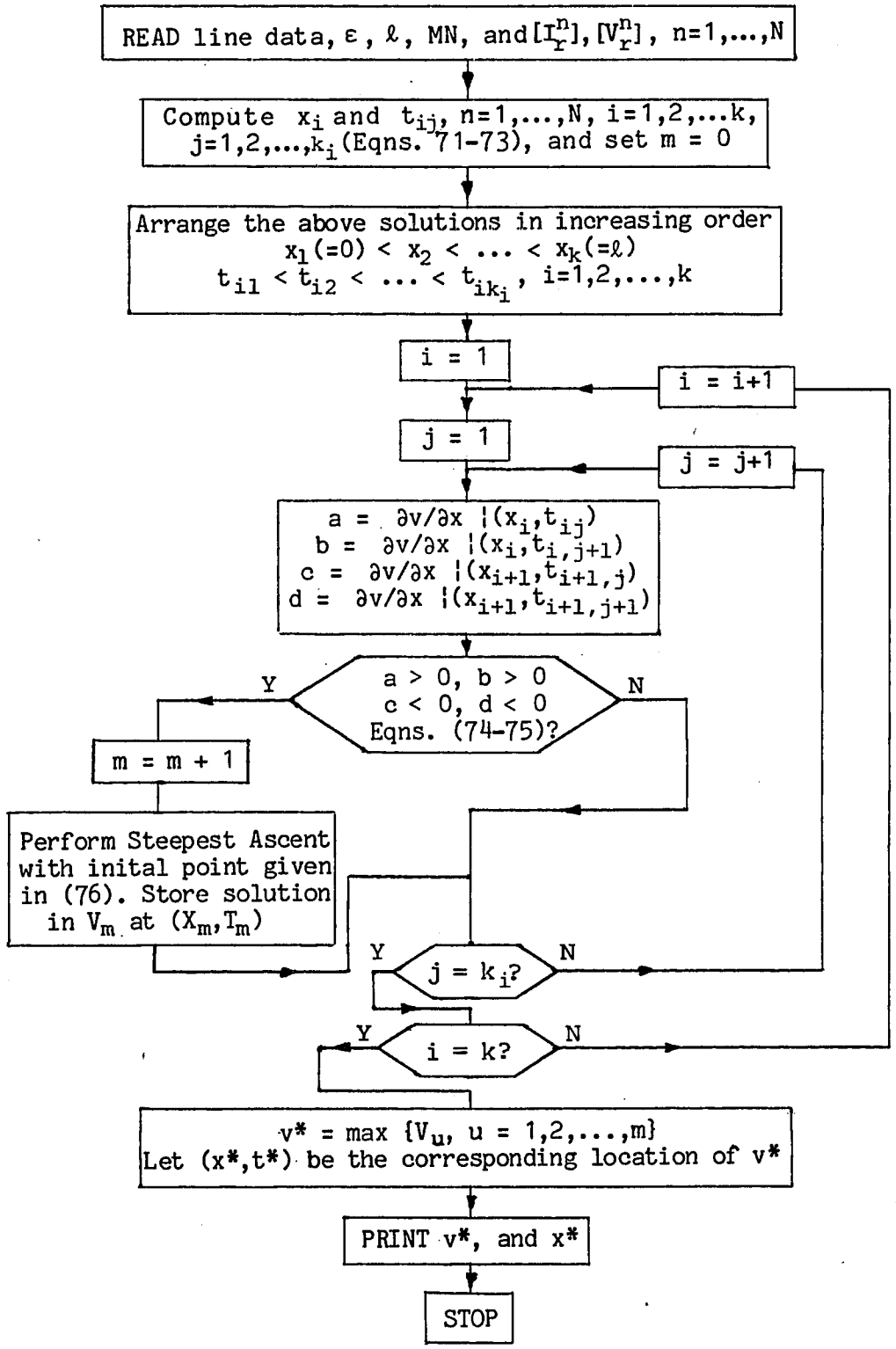

Fig. 18. Flowchart for Computing Maximum Peak Voltage.

5.4 Maximum Distortion Factor

Other applications of the proposed method include the determination of the global maxima of voltage and current distortion factors which are of interest in verifying whether the harmonic levels conform with existing recommended standards. The distortion factor squared of the current flowing in phase k is given by

$$(DF)^2 = \{ \sum_{n=2}^{N} (I_k^n)^2 \}/(I_k^1)^2. \tag{80}$$

Note that the rate of change in the rms value of the fundamental current with distance x may be considered to be negligible when compared to those of the higher order harmonic currents. Hence, when applying the global convergence method to (80), a Lipschitz constant may be taken to be the sum of L_k^n, n=2,...,N. Because of the fact that $(DF)^2$ is also unimodal in each of the intervals defined by the set of points given by (66), the local convergence method may also be applied to (80) in the same way as in finding the local maxima of the total rms current.

Both the global and local convergence methods can also be used to determine the maximum distortion factor of the phase or line voltage. The rms values of these signals needed in (80) may be directly obtained from (69) and (78).

5.5 Single-Phase Lines

The corresponding solutions of the voltage and current wave equations of a single-phase transmission line are respectively given by

$$\bar{V}^n = \bar{V}^{n+}\exp(\bar{\gamma}^n x)+\bar{V}^{n-}\exp(-\bar{\gamma}^n x) = V^n(x)\exp\{j\psi^n(x)\} \tag{81}$$

and

$$\bar{I}^n = \bar{I}^{n+}\exp(\bar{\gamma}^n x) + \bar{I}^{n-}\exp(-\bar{\gamma}^n x) \tag{82}$$

where

$$\bar{V}^{n\pm} = \frac{1}{2}(\bar{V}_r^n \pm \bar{I}_r^n \bar{Z}_c^n) = V^{n\pm} \exp(j\delta^{n\pm}),$$

$$I^{n\pm} = \frac{1}{2}(\bar{I}_r^n \pm \bar{V}_r^n/\bar{Z}_c^n) = I^{n\pm} \exp(j\theta^{n\pm}).$$

Herein,

$$\bar{Z}_c^n = \sqrt{\bar{z}^n/\bar{y}^n}$$

and

$$\bar{\gamma}^n = \sqrt{\bar{z}^n \bar{y}^n} .$$

The variations of the series impedance $\bar{z}^n$ and shunt admittance $\bar{y}^n$ with frequency are illustrated in Appendix II.

From Eqn. (82), the total rms current squared is found to be [69]

$$I^2(x) = \sum_{n=1}^{N} \{[I^{n+}\exp(\alpha^n x)]^2+[I^{n-}\exp(-\alpha^n x)]^2+2I^{n+}I^{n-}\cos(\theta^{n+}-\theta^{n-}+2\beta^n x)\}. \quad (83)$$

If the extrema of the rms of a single harmonic current of order n are of interest, then only the expression for one single harmonic from (83) is needed:

$$I^{n2}(x) = [I^{n+}\exp(\alpha^n x)]^2+[I^{n-}\exp(-\alpha^n x)]^2+2I^{n+}I^{n-}\cos(\theta^{n+}-\theta^{n-}+2\beta^n x) \quad (84)$$

For power system transmission lines, α^n is small for all harmonic frequencies of concern. Therefore, the exponentials in (84) may be approximated by unity for normal line lengths. Then equating the derivative of (84) with respect to x to zero yield the locations for rms current extrema:

$$x_m = \frac{\theta^{n-} - \theta^{n+} + m\pi}{2\beta^n}, \qquad m = \begin{cases} \text{even for maximum} \\ \text{odd for minimum} \end{cases} \quad (85)$$

for x_m less than the line length. Note that the maximum rms current locations given in (85) agree with those found in Ref. [20]. The value of maximum rms current is then computed by taking the square root of (84) evaluated at x_m from (85) with m even.

For the total rms current, however, it can be readily seen that applying the above procedure to Eqn. (84) would result in a complicated transcendental equation for which a closed form solution is not available. Hence, an iterative numerical method is needed to generate the solution. The global and local convergence algorithms discussed previously can be readily used to determine the global maximum of (84). the Lipschitz constant required by the algorithm in Fig. 16 is accurately computed by

$$|dI^2/dx| = \sum_{n=1}^{N} 2(\alpha^n W^n + 2\beta^n I^{n+} I^{n-}) \triangleq L \tag{86}$$

where

$$W^n = \max\{|(I^{n+})^2 - (I^{n-})^2|,\ |(I^{n+})^2 \exp(2\alpha^n \ell) - (I^{n-})^2 \exp(-2\alpha^n \ell)|\}.$$

On the other hand, the points on the transmission line which determine the regions of unimodality required by the algorithm in Fig. 15 are determined by equation (66).

With regard to locating the maximum peak voltage of the overall instantaneous voltage derived from (81), i.e.,

$$v(x,t) = \sqrt{2} \sum_{n=1}^{N} V^n(x) \sin\{n\omega_o t - \psi^n(x)\}, \tag{87}$$

the algorithm in Fig. 18 can also be readily used. This is accomplished by computing both the specific line locations by (71)-(72), and the time instants by (73) that both determine the regions in the x-t plane where v(x,t) is guaranteed to have at most one maximum.

5.6 Numerical Example and Discussion of Results

The objective of this example is to illustrate the effectiveness of the procedure for computing the maximum values of the rms current, peak

voltage and distortion factor. Let a study be conducted on a 150-mile long three-phase untransposed transmission line whose geometry is shown in Fig. 19.

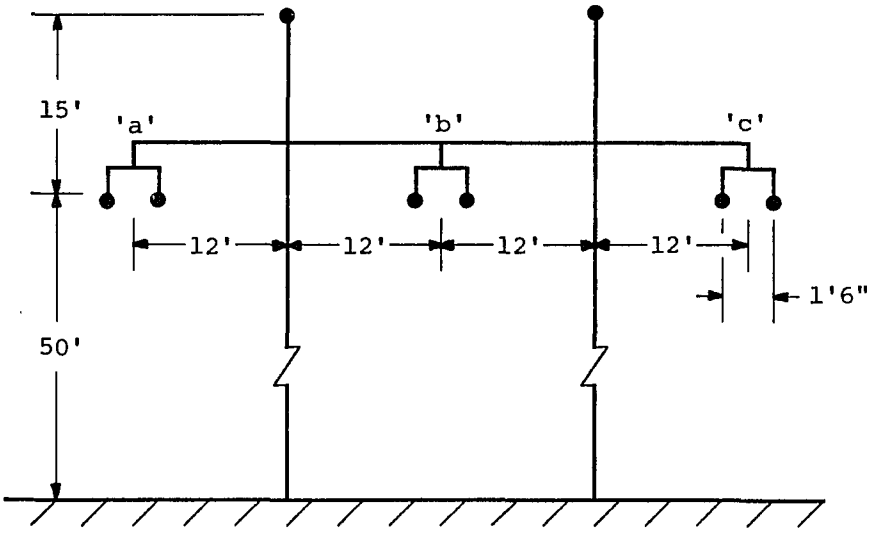

Fig. 19. Three-Phase Transmission Line (Phase Wires: 795000 CM 26/7 ACSR; Steel Ground Wires: R = 4 /mi and GMR = 0.001 ft).

The voltage and current harmonic levels at the receiving end of the line listed in Table II may not be representative of an actual transmission system. However, unbalanced as well as uncharacteristic harmonics, both of which were reported in practice, are taken into account with their phase angles are random. The per-unit values of the phase voltage and current fundamentals (based on 100 MVA and 345 kV) were taken to be $\bar{V}_a^1 = 1\angle 0^\circ$, $\bar{V}_b^1 = 1\angle -120^\circ$, $\bar{V}_c^1 = 1\angle 120^\circ$, $\bar{I}_a^1 = 2\angle 13^\circ$, $\bar{I}_b^1 = 2\angle -115^\circ$, and $\bar{I}_c^1 = 2\angle 123^\circ$.

Data preparation for using the algorithms is initiated by finding the impedance and admittance matrices at each harmonic frequency as reviewed in Appendix II. Then, the eigenvalues and eigenvectors of the matrix product $[\bar{Y}^n][\bar{Z}^n]$ are computed by a standard IMSL subroutine. The

following simulation results were obtained by using the flowcharts of Figs. 16, 17 and 18.

TABLE II
HARMONIC LEVELS (% OF FUNDAMENTALS) AND THEIR PHASE ANGLES (DEGREES W.R.T. V_a^1) AT RECEIVING LINE END

n	$\bar{V}_a^n$		$\bar{V}_b^n$		$\bar{V}_c^n$		$\bar{I}_a^n$		$\bar{I}_b^n$		$\bar{I}_c^n$	
3	2.7	112	2.5	-9	2.5	-31	4.9	112	4.7	55	5.1	32
5	2.3	72	2.4	30	2.0	88	3.8	-14	3.6	-133	3.6	-84
7	1.5	153	1.3	75	1.4	-160	3.0	-166	3.2	3	2.5	29
9	1.2	-123	0.5	125	0.9	-84	2.5	54	2.9	104	2.4	-100
11	0.6	-43	0.6	-164	0.6	-4	2.1	-66	2.4	-159	1.6	133
13	0.4	108	0.5	111	0.6	75	1.4	87	1.8	21	1.2	-45
15	4.4	54	0.4	-121	0.3	26	1.0	10	1.2	66	1.1	-121
17	2.1	-20	3.0	-42	1.2	168	4.2	173	4.7	138	3.9	81
19	1.8	-143	2.0	-20	1.0	131	4.8	-49	3.3	-9	2.9	-61
21	0.3	176	0.3	54	3.0	-143	0.5	-172	0.8	-150	1.6	-138
23	0.1	11	0.2	-91	0.2	-33	0.2	47	0.5	147	1.5	73
25	1.3	-122	1.5	56	2.5	53	4.5	96	3.8	-70	5.2	174
27	1.7	-6	1.2	177	1.6	-173	5.0	-108	5.0	59	4.0	16
29	0.5	22	0.5	2	0.0	17	0.2	37	0.3	-30	0.1	-43

The computed results are summarized in Table III which lists the number of local maxima, M, (excluding the line boundaries), the magnitudes and locations of global maxima of the rms currents, peak voltages and distortion factors. The local convergence method required an average of only 15 iterations for each local maximum of rms currents or distortion factors with a tolerance of 0.01. The global convergence method converged to the global maximum of each objective function with an average of 46 iterations using the same tolerance.

In computing the local maxima of the phase and line voltages, there were approximately 9530 regions where the gradient was computed for possible local maxima. Only M of these as listed in Table III satisfied the necessary and sufficient condition of local maxima. Then the

steepest ascent method using a fixed step size required an average of 17 iterations per local maximum with the same tolerance of 0.01.

TABLE III
COMPUTED GLOBAL MAXIMA AND LOCATIONS OF RMS CURRENTS, PEAK VOLTAGES AND DISTORTION FACTORS

	RMS Current & Peak Voltage			Distortion Factor		
	M	Mag.(pu)	Loc.(mi)	M	Mag.(pu)	Loc.(mi)
I_a	2	2.024	59.83	2	12.17	0.00
I_b	3	2.020	63.64	2	11.80	0.00
I_c	3	2.026	62.10	3	11.34	1.56
V_a	17	1.89	114.02	2	21.11	118.35
V_b	18	1.74	135.09	2	21.74	150.00
V_c	16	1.74	38.25	2	19.94	97.17
V_{ab}	14	1.64	28.83	3	12.87	84.12
V_{bc}	12	1.55	88.38	3	8.99	35.47
V_{ca}	13	1.78	146.72	3	12.36	137.36

To verify the results of Table III, the total rms currents, peak voltages and distortion factors were computed for all points of the transmission line with an increment of .01 mile. The results are shown in Figs. 20, 21 and 22, respectively. The global and local maxima as well as their locations coincide with those listed in Table III.

Note that not all the local maxima of the peak voltages can be observed in Fig. 21. To see all the local maxima in the search region, a three-dimensional plot of the instantaneous voltages is necessary as shown in Fig. 23 for phase 'a' voltage at $\pm 1/6f_o$ seconds from the time when the fundamental component reaches its maximum.

From the results of this example, it is recognized that the variation between the minimum and maximum rms current is not appreciable. In this case the variation of heating along the lines is insignificant.

For the maximum peak voltage, however, the difference between the maximum and minimum peak values could not be ignored.

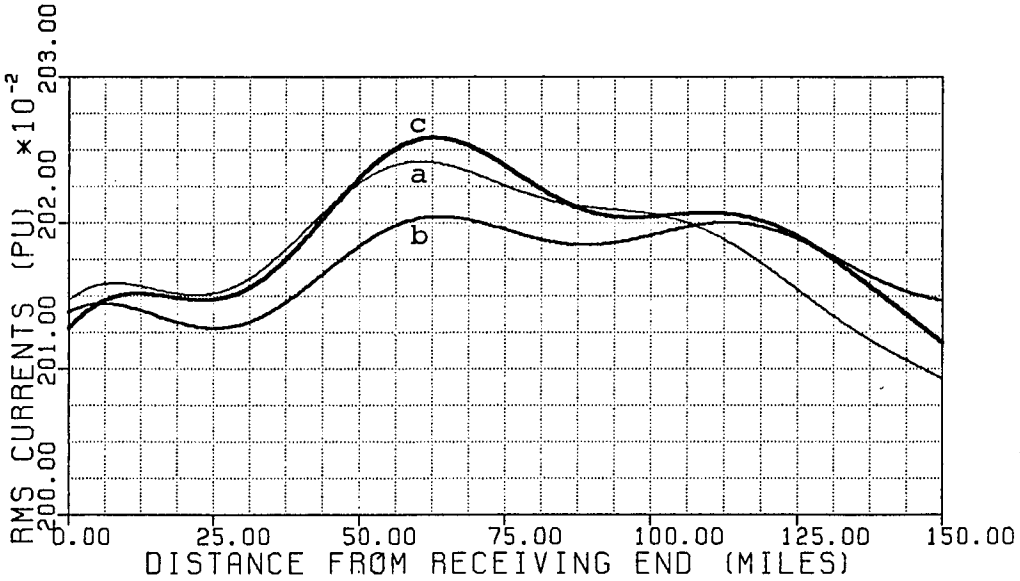

Fig. 20. Variation of RMS Currents.

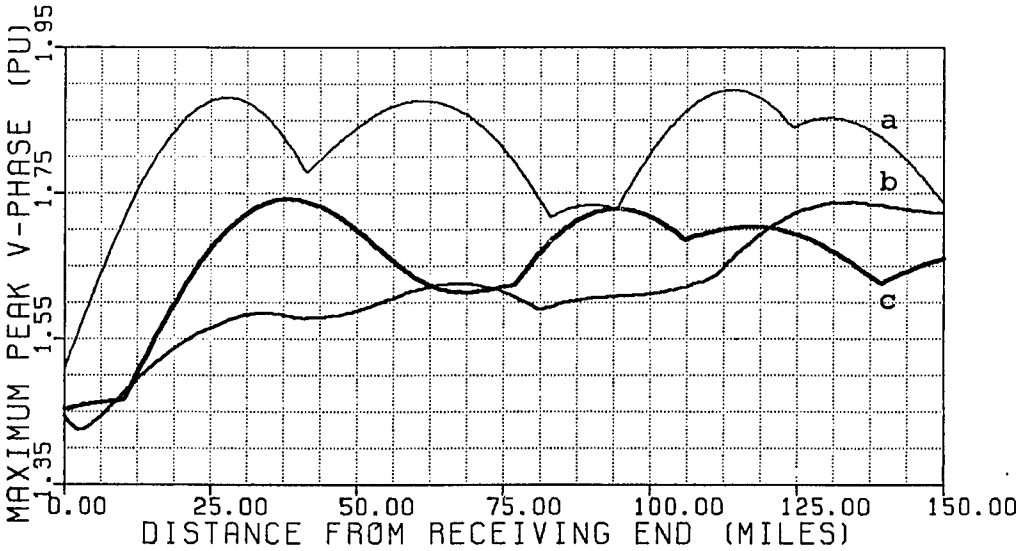

(a)

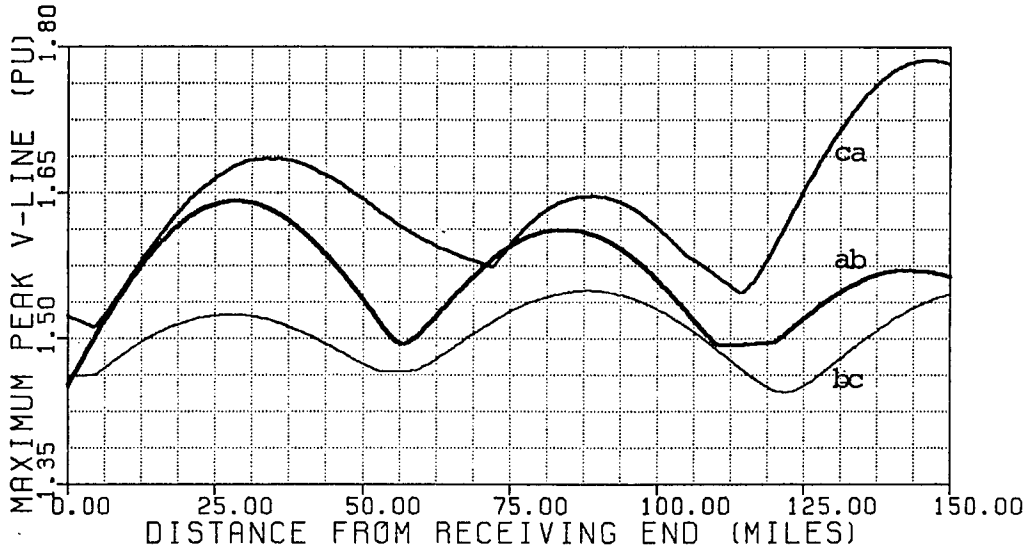

(b)

Fig. 21. Variation of Peak (a) Phase Voltages and (b) Line Voltages.

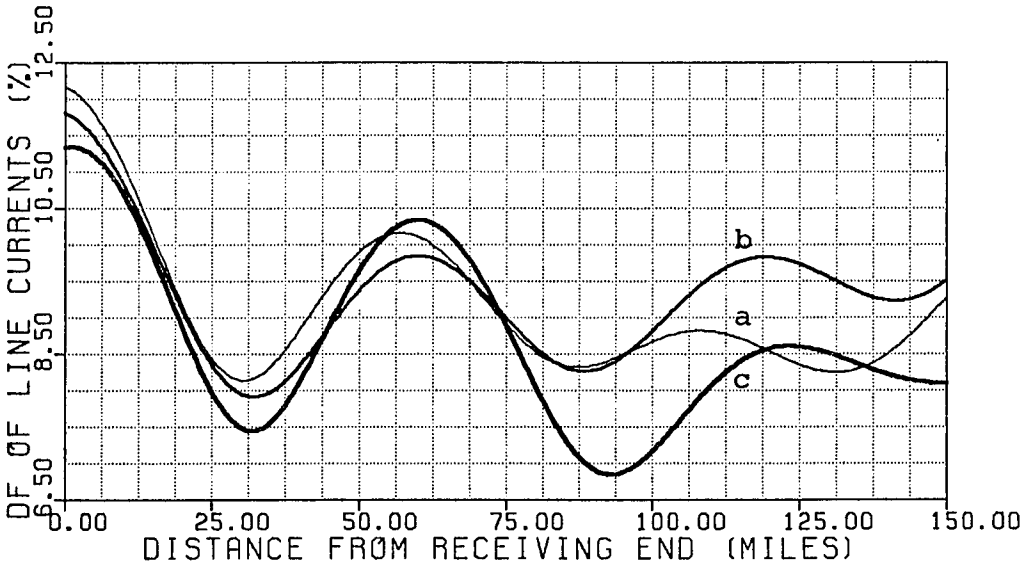

(a)

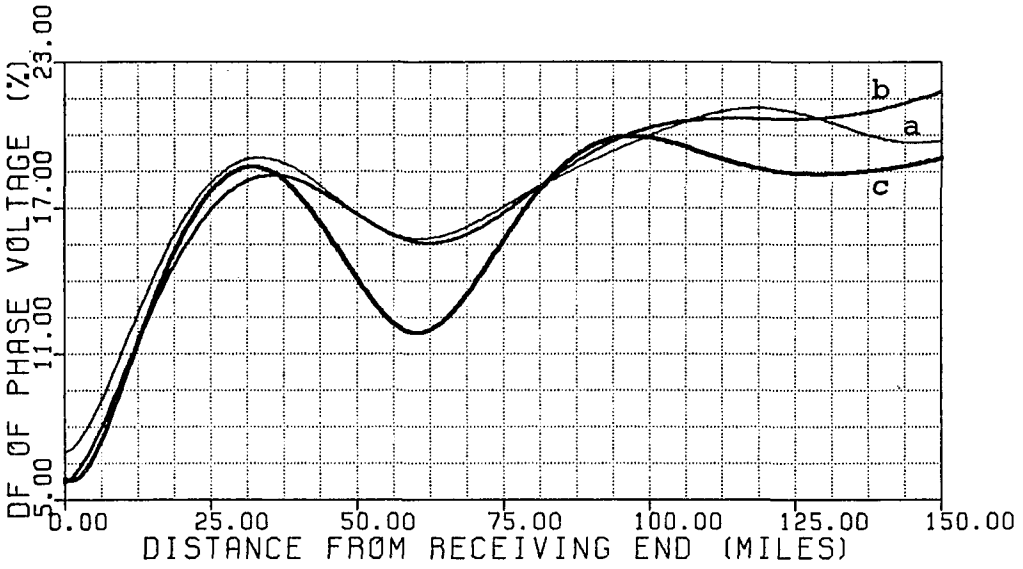

(b)

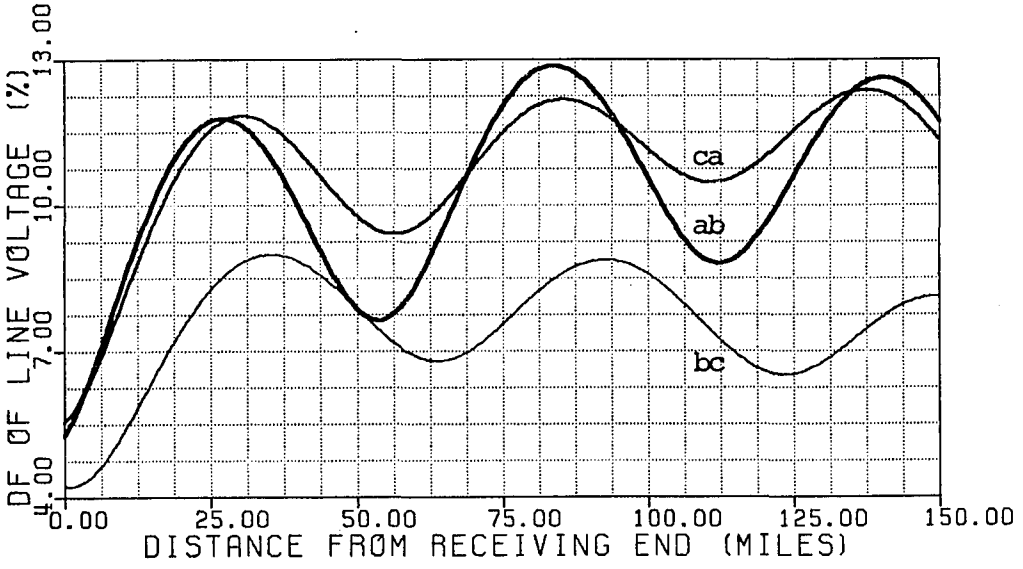

(c)

Fig. 22. Distortion Factor of (a) Currents, (b) Phase Voltages and (c) Line Voltage.

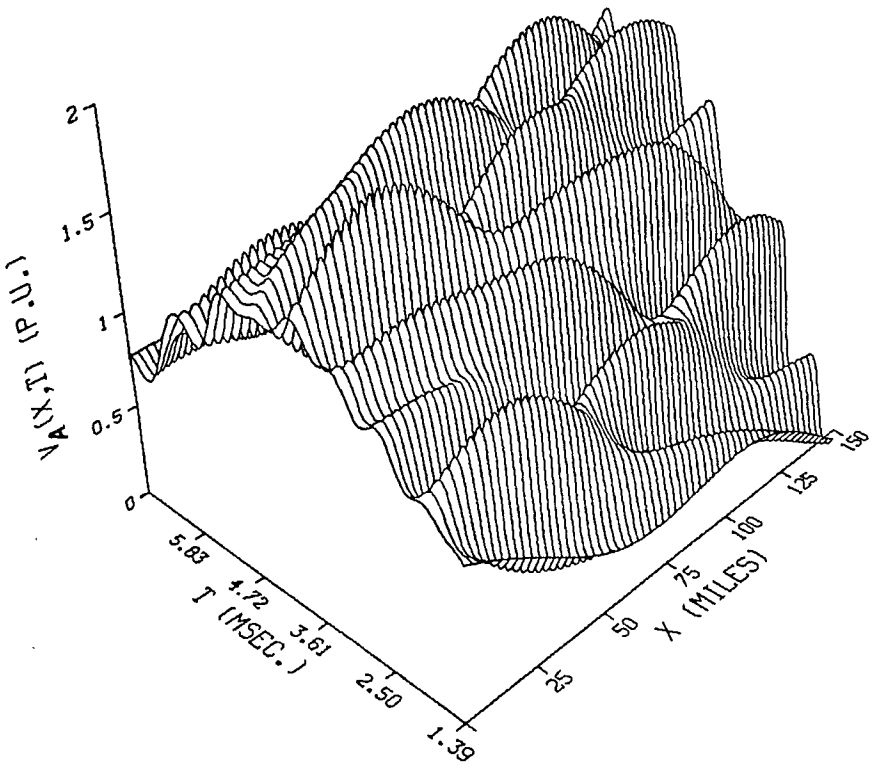

Fig. 23. Instantaneous Phase a Voltage in Search Region.

6. CONCLUSIONS

With the rapidly increasing application of static power converters, harmonic levels in power and distribution systems are becoming intolerable, thus leading to an increasing number of failures of some components and degrading the performance of some others. Furthermore, longer telephone loops and the rapid growth of digital-data transmission devices may lead to inductive communication interference. Therefore, an urgent need of novel or improved methods has developed for harmonic analysis and mitigation.

The major contribution of the work presented in this dissertation includes the following:

1. In cases where nonlinear loads are randomly varying, a practical method has been presented for probabilistic modeling of harmonic voltages and currents. The resulting probability characteristics of the random signals represent a more realistic description of harmonics in power systems. The principal application of the probabilistic model is for developing harmonic standards where probability measures should be assigned to maximum permissible limits.
2. Considering that the -equivalent model of a transmission line only provides information at the line terminals, efficient numerical methods are presented to compute and locate the global maximum of any single voltage or current harmonic, overall peak voltage, total rms current and distortion factors. Since these maxima may create hot spots, insulation damage or communication interference, their prediction is important when harmonic limitations at the transmission level are to be observed.

Recommendations for future research efforts on power system harmonics include

- Identifying improved or new methods for harmonic control.
- Quantitatively determining harmonic effects on system components.
- Searching for improved methods of harmonic analysis.
- Relaxing some of the assumptions made for the probabilistic harmonic modeling.
- Assessing harmonic effects on power system dynamic stability.

Finally, it is the author's opinion that sufficient coverage of the harmonic problems should be given in a power electronics course.

REFERENCES

[1] C. R. Clinker, "Harmonic Voltages and Currents in 'Wye' and 'Delta' Transformer Connections," **AIEE Trans.**, Vol. 33, 1914, pp. 723-33.

[2] R. P. Stratford, "Harmonic Pollution in Power Systems - A Change in Philosophy," **IEEE Trans. Ind. Appl.**, Vol. 16, No. 5, 1980, pp. 617-23.

[3] Electric Power Research Institute (EPRI), **Distribution System Surge and Harmonic Characteristics**, Final Report, Nov. 1980, EPRI EL-1627, RP 1024-1, prepared by McGraw-Edison Co., United Technologies Corp. and Systems Control Inc.

[4] J. Arrillaga, D. A. Bradly and P. S. Bodger, **Power Systems Harmonics**, John Wiley & Sons, 1985.

[5] A. A. Mahmoud (Ed.), **Power System Harmonics**, IEEE Tutorial Course, No. 84 EH0221-2-PWR, 1984.

[6] Y. Baghzouz and Owen T. Tan, "Harmonic Analysis of Induction Watthour Meter Performance," **IEEE Trans. Power App. and Syst.**, Vol. PAS-102, No. 2, 1985, pp. 399-406.

[7] W. F. Horton and S. Goldberg, "The Effect of Harmonics on the Operating Points of Electromechanical Relays," **IEEE Trans. Power App. and Syst.**, Vol. PAS-104, No. 5, 1985, pp. 1178-88.

[8] A. M. Sharaf, "Harmonic Interference from Distribution Systems," **IEEE Trans. Power App. and Syst.**, Vol. PAS-101, No. 8, 1982, pp. 2975-81.

[9] IEEE Working Group on Power System Harmonics, "Power Line Effects on Communication Interference," **IEEE Trans. Power App. and Syst.**, Vol. PAS-104, No. 9, 1985, pp. 2578-87.

[10] M. F. McGranaghan, J. H. Shaw and R. E. Owen, "Measuring Voltage and Current Harmonics on Distribution Systems," **IEEE Trans. Power App. and Syst.**, Vol. PAS-100, No. 7, 1981, pp. 3599-608.

[11] G. D. Breuer, G. Addis, R. H. Lassater and J. J. Vithayathil, "HVDC-AC Harmonic Interaction, Part II: AC System Model with Comparison of Calculated and Measured Data," **IEEE Trans. Power App. and Syst.**, Vol. PAS-101, No.3, 1982, pp. 709-18.

[12] D. J. Pileggi, N. H. Chandra and A. E. Emanuel, "Prediction of Harmonic Voltages in Power Systems," **IEEE Trans. Power App. and Syst.**, Vol. PAS-100, No. 3, 1981, pp. 1307-15.

[13] A. A. Mahmoud and R. D. Shultz, "A Method for Analyzing Harmonic Distribution in AC Systems," **IEEE Trans. Power App. and Syst.**, Vol. PAS-101, No. 6, 1982, pp. 1815-24.

[14] D. Xia and G. T. Heydt, "Harmonic Power Flow Studies, Part I: Formulation and Solution, and Part II: Implementation and Practical Application," **IEEE Trans. Power App. and Syst.**, Vol. PAS-101, No. 6, 1982, pp. 1257-70.

[15] IEEE Working Group on Power System Harmonics, "Power System Harmonics: An Overview," **IEEE Trans. Power App. and Syst.**, Vol. PAS-102, No. 8, 1983, pp. 2455-60.

[16] A. E. Emanuel., J. A. Orr and D. Cyganski, "The need of Collection of Actual Data on Voltage and Current Harmonics," **Proc. IEEE IAS Annual Meeting**, Chicago, Illinois, Sept. 30 - Oct. 4, 1984, pp. 380-6.

[17] John A. Orr, Alexander E. Emanuel and David G. Pileggi, "Current Harmonics, Voltage Distortion and Powers Associated with Electric Vehicle Battery Chargers Distributed on the Residential Power System," **IEEE Trans. Ind. Appl.**, Vol. IA-20, No. 4, 1984, pp. 727-734.

[18] R. DeVre, "Harmonic Distortion Produced in Supply Networks by Television Receivers and Light Dimmers," **IEE Conf. Pub.**, No. 210, 1981, pp. 121-8.

[19] A. E. Emanuel and S. R. Kaprielian, "Contribution to the Theory of Stochastically Periodic Harmonics in Power Systems," **IEEE PES, Winter Meeting**, New York, Feb. 2-7, 1986, Paper No. 86 WM 164-8.

[20] R. D. Shultz, R. A. Smith and G. L. Hickey, "Calculation of Maximum Harmonic Currents and Voltages on Transmission lines," **IEEE Trans. Power App. Syst.**, Vol. PAS-102, No. 4, 1983, pp. 817-21.

[21] P. M. Anderson, **Analysis of Faulted Power Systems**, Iowa State University Press, Ames, Iowa, 1976.

[22] Y. Baghzouz and Owen T. Tan, "Harmonics in Distribution Systems," **Proc. 35th Annual Conf. for Protective Relay Engrs.**, Texas A&M University, 1982, pp. 1-17.

[23] E. W. Kimbark, **Direct Current Transmission**, John Wiley and Sons, New York, 1971.

[24] IEEE Power System Harmonics Working Group, "Bibliography on Power System Harmonics, Parts I & II," **IEEE Trans. Power App. and Syst.**, Vol. PAS-103, No. 9, 1984, pp. 2460-79.

[25] P. P. Biringer and M. A. Slonim, "Determination of Harmonics of Converter Current and/or Voltage Waveforms (New Method of Fourier Series Coefficients), Parts I & II," **IEEE Trans. Ind. Appl.**, Vol. IA-16, No. 2, 1980, pp. 242-53.

[26] J. W. Cooley and J. W. Tukey, "An Algorithm for the Machine Calculation of Complex Fourier Series," **Mathematics of Computations**, Vol. 19, April 1965, pp. 297-301.

[27] IEEE Std 519-1981, **Guide for Harmonic Control and Reactive Compensation of Static Power Converters**, IEEE Publication, 1981.

[28] T. Subbarao and J. Reeve, "Harmonics Caused by Imbalanced Transformer Impedances and Imperfect Twelve-Pulse Operation in HVDC Conversion," **IEEE Trans. Power App. and Syst.**, Vol. PAS-95 No. 5, 1976, pp. 1732-7.

[29] A. D. Graham and E. T. Schonholzer, "Line Harmonics of Converters with D.C. Motor Loads," **IEEE Trans. Ind. Appl.**, Vol. IA-19, No. 1, 1983, pp. 84-93.

[30] R. L. Smith and R. P. Stratford, "Power System Harmonics from Adjustable-Speed Drives," **IEEE Trans. Ind. Appl.**, Vol. IA-29, No. 4, 1984, pp. 973-77.

[31] J. A. Orr, A. E. Emanuel and D. J. Pileggi, "Current Harmonics, Voltage Distortion, and Powers Associated with Battery Chargers, Part I: Comparisons Among Different Types of Chargers," **IEEE Trans. Power App. and Syst.**, Vol. PAS-101, No. 8, 1982, pp. 2703-10.

[32] A. K. Wallace, E. S. Ward and A. Wright, "Sources of Harmonic Currents in Slip-Ring Induction Motors," **Proc. IEE**, Vol. 121, No. 12, 1974, pp. 1495-1500.

[33] T. J. E. Miller, **Reactive Power Control in Electric Systems**, John Wiley & Sons, 1982.

[34] G. Goldberg, "Behavior of Apparatus under the Influence of Voltage and Current Harmonics," **Bull. Soc. R. Belge Electr.**, Vol. 91, No. 4, 1975, pp. 225-35.

[35] W. S. Wood, F. P. Flynn and A. Poray, "Effects of Supply Voltage Waveform Distortion on Motor Performance," **Int. Conf. on Sources and Effects of Power System Disturbances**, London , England, April 1974, pp. 261-7.

[36] Electric Power Research Institute (EPRI), **Evaluation of Electrical Interference to the Induction Watthour Meter**, EL-2315, Research Project No. 1738, Final Report, April 1982.

[37] IEEE Power System Relaying Committee, **Sine-Wave Distortion in Power Systems and the Impact on Protective Relaying**, Final Report, 84 TH 0115-6 PWR, 1984.

[38] W. Shepherd and P. Zand, **Energy Flow and Power Factor in Nonsinusoidal Circuits**, Cambridge University Press, England, 1979.

[39] H. Sasaki and T. Machida, "A new Method to Eliminate AC Harmonics by Magnetic Flux Compensation," **IEEE Trans. Power App. and Syst.**, Vol. PAS-100, No. 11, 1971, pp. 2009-19.

[40] A. Aminati, "Generalized Method of Harmonic Reduction in AC/DC converters by Harmonic Current Injection," **Proc. IEE**, Vol. 119, No. 7, 1972, pp. 857-64.

[41] H. S. Patel and R. G. Hoft, "Generalized Techniques of Harmonic Elimination and Voltage Control in Thyristor Inverters: Part I - Harmonic Elimination," **IEEE Trans. Ind. Appl.**, Vol. IA-10, No. 3, 1973, pp. 310-17.

[42] J. F. Baird an J. Arrillaga, "Harmonic Reduction in D. C. Ripple Reinjection," **Proc. IEE**, Vol. 127, Pt. C, No. 3, 1980, pp. 294-303.

[43] M. F. McGranaghan R. C. Dugan, J. A. King and W. T. Jewell, "Distribution Feeder Harmonic Study Methodology," **IEEE Trans. Power App. and Syst.**, Vol. PAS-103, No. 12, 1984, pp. 3663-71.

[44] Electric Power Research Institute (EPRI), **Harmonic Power Flow Studies, Vol. 1: Theoretical Basis**, EL-3300, Project No. 1764-7, Prepared by Purdue University, Final Report, November, 1983.

[45] W. M. Grady and G. T. Heydt, "Prediction of Power System Harmonics Due to Gaseous Discharge Lighting," **IEEE PES Summer Meeting**, Seattle, Washington, July 15-20, 1984, paper No. 84 SM 555-9.

[46] G. L. Kusic and I. A. Whyte, "Three-Phase Steady State Static VAR Generator Filter Design for Power Systems," **IEEE Trans. Power App. and Syst.** , Vol. PAS-103, No. 4., 1984, pp. 811-18.

[47] B. Szabados and J. Lee, "Harmonic Impedance Measurements on Transformers," **IEEE Trans. Power App. and Syst.**, Vol. PAS-100, No. 12, 1981, pp. 5020-26.

[48] Owen T. Tan and P. Hillers, **Power System Harmonic Analysis**, Technical Report prepared for Louisiana Power and Light Co., Louisiana State University, Baton Rouge, Louisiana, September, 1981.

[49] R. H. Kitchin, "New Method of Digital Computer Evaluation of Converter Harmonics in Power Systems Using State-Variable Analysis," **Proc. IEE**, Vol. 128, Pt. C, No. 4, 1981, pp. 196-206.

[50] B. T. Coi, N. Menemenlis and H. L. Nakra, "Fast Steady-State Solution for HVDC Analysis," **IEEE Trans. Power App. and Syst.**, Vol. PAS-99, No. 6, 1980, pp. 2453-59.

[51] S. Williams and I. R. Smith, "Fast Digital Computation of Three-Phase Thyristor Bridge Circuits," **Proc. IEE**, Vol. 120, No. 7, 1973, pp. 791-95.

[52] G. Stagg and A. El-Abiad, **Computer Methods in Power System Analysis**, McGraw-Hill Book Co., New York, 1968.

[53] M. F. McGranaghan, R. C. Dugan and W. L. Sponsler, "Digital Simulation of Distribution System Frequency Response Characteristics," **IEEE Trans. Power App. and Syst.**, Vol. PAS-100, No. 3, 1981, pp. 1362-9.

[54] W. G. Sherman, "Summation of Harmonics with Random Phase Angles," **IEE Proc.**, Vol. 119, No. 11, 1972, pp. 1643-8.

[55] N. B. Rowe, "The Summation of Randomly Varying Phasors or Vectors with Particular Reference to Harmonic Levels," **IEE Conf. Pub.**, No. 210, 1981, pp. 121-8.

[56] A. Kloss, "Statistical Analysis of Harmonic Problems in Power Electronic Installations," **Bull. Assoc. Suises Electr.**, Vol. 66, No. 8, 1975, pp. 427-33.

[57] Y. Baghzouz and Owen T. Tan, "Probability Distribution of the Summation of Random Power System Harmonics," **Proc. IEEE SOUTHEASTCON.**, Raleigh, NC, March 31 - April 3, 1985, pp. 39-44.

[58] R. E. Morrison and A. D. Clark, "Probabilistic Representation of Harmonic Currents in AC Traction Systems," **Proc. IEE**, Vol. 131, No. 5, 1984, pp. 181-9.

[59] Y. Baghzouz and Owen T. Tan, "Probabilistic Modeling of Power System Harmonics," **IEEE I&CP Technical Conference**, Cleveland, Ohio, May 5-8, 1986. (Also considered for publication in IEEE Trans. on Industry Applications)

[60] J. A. Orr, D. Cyganski, A. E. Emanuel and R. T. Saleh, "Design of a System for Automated Measurement and Statistics Calculation of Voltage and Current Harmonics," **IEEE PES, Winter Meeting**, New York, Feb. 2-7, 1986, Paper No. 86 Wm 198-6.

[61] Paul G. Hoel, Sidney C. Port and Charles J. Stone, **Introduction to Probability Theory**, Houghton Miffin Co., 1971

[62] H. J. Nussbaumer, **Fast Fourier Transform and Convolution Algorithms**, Heidelberg, Germany, Springer Verlag, 1982.

[63] R. Agarwal and J. W. Cooly, "New Algorithms for Digital Convolution," **IEEE Trans. on ASSP**, Vol. 25, No. 5, 1977, pp. 392-410.

[64] P. M. Anderson and A. Bose, "A Probabilistic Approach to Power System Stability Analysis," **IEEE Trans. Power App. and Syst.**, Vol. PAS-102, No. 8, 1983, pp. 2430-39.

[65] R. N. Allan and A. M. Leite da Silva, "Probabilistic Load Flow Using Multi-Linearization," **Proc. IEE**, Vol. 128, Pt. C, No. 5, 1981, pp. 280-87.

[66] J. Griffin, "Fluorescent Lamps, Neutral Currents and Standby Generators," **Electrical Review**, Vol. 204, Jan. 1979, pp. 21-2.

[67] T. L. Baitch, "The Australian Standard to Specify Network Harmonic Limits: AS 2279-1979," **IEEE Trans. Ind. Appl.**, Vol. IA-18, No.3, 1982, pp.260-7.

[68] The Electricity Council, **Limits for Harmonics in the United Kingdom Electricity Supply System**, Recommendation G5/3, London, Sept. 1976.

[69] Y. Baghzouz and Owen. T. Tan, "Computation of Maximum RMS Current and Peak Voltage on Transmission Lines under Nonsinusoidal Conditions," **IEEE PES Winter Meeting**, New York, Feb. 2-7, 1986, Paper No. 86 WM 153-1.

[70] J. Arrillaga, T. J. Densem and B. J. Harker, "Zero Sequence Harmonic Current Generation in Transmission Lines Connected to a Large Converter Plant," **IEEE Trans. Power App. and Syst.**, Vol. PAS-102, No. 7, 1983, pp. 2357-63.

[71] T. J. Densem, P. S. Bodger and J. Arrillaga, "Three Phase Transmission System Modeling for Harmonic Penetration Studies," **IEEE Trans. Power App. Syst.**, Vol. PAS-103, No. 2, 1984, pp. 310-17.

[72] Y. Baghzouz and Owen T. Tan, "Maximum Heating and Insulation Stress on Untransposed Transmission Lines with Unbalanced Harmonic Distortion," **IEEE PES Summer Meeting**, July 20-25, 1986, Mexico City, Mexico, paper No. GS 10 SPM-86.

[73] Bruno O. Shubert, "A Sequential Method Seeking the Global Maximum of a Function," **SIAM Journal of Numerical Analysis**, Vol. 9, No. 3, Sept. 1972, pp. 379-88.

[74] M. Chen and W. E. Dillon, "Power System Modeling," **Proc. IEEE**, Vol. 62, No. 7, 1974, pp. 901-15.

[75] W. I. Bowman and J. M. McNamee, "Development of Equivalent Pi and T Matrix Circuits for Long Untransposed Transmission Lines," **IEEE Trans. Power App. Syst.**, Vol. PAS-84, No. 6, 1964, pp. 625-32.

[76] S. S. Rao, **Optimization Theory and Applications**, Wiley Eastern Limited, 1984.

APPENDIX I

HARMONIC COMPUTATION OF DISTORTED WAVEFORMS

The Fourier series of a periodic function w(t) with period T is given by

$$w(t) = W_o + \sum_{n=1}^{\infty} \{a_n \cos(n\omega t) + b_n \sin(n\omega t)\} \tag{A.1}$$

where

$$W_o = \frac{1}{T} \int_0^T w(t)\, dt$$

$$a_n = \frac{2}{T} \int_0^T w(t) \cos(n\omega t)\, dt$$

$$b_n = \frac{2}{T} \int_0^T w(t) \sin(n\omega t)\, dt$$

and $\omega = 2\pi/T$. Equation (A.1) may be rewritten in the following form:

$$w(t) = W_o + \sum_{n=1}^{\infty} \{W_n \cos(n\omega t + \phi_n\} \tag{A.2}$$

where

$$W_n = (a_n^2 + b_n^2)^{\frac{1}{2}}$$

and

$$\phi_n = \arctan(b_n/a_n).$$

In general, voltage and current waveforms found in power systems are rotational symmetric. Then, (A.2) reduces to

$$w(t) = \sum_{n=1,3,5,\ldots}^{\infty} W_n \cos(n\omega t + \phi_n). \tag{A.3}$$

The current and voltage waveforms found in converter installations are generally discontinuous several times per period due SCR switchings. The repetitive integrations for each interval where the voltage or current is continuous may then be avoided by using the complex form of Fourier series. In such cases, the Fourier coefficients are generally

determined by the jumps of the function and its derivatives at the points of discontinuities [25].

Another application of the complex Fourier series is when the available data are given in discrete form. If a periodic function w(t) is sampled m times per period, then assuming that w(t) is linear between consecutive sampling points, the Fourier coefficients are computed by

$$a_n - jb_n = \frac{-2}{Tn^2\omega^2} \sum_{i=1}^{m-1} \delta_i \exp(-jn\omega t_i) \qquad (A.4)$$

where δ_i is the jump of the derivative of w(t) at sampling time t_i. From (A.4), it is clear that the Fourier coefficients can be evaluated by algebraic addition rather than integration, thereby reducing the computational effort.

Another well known algorithm for computing the complex Fourier series of a signal given in discrete form is the Fast Fourier Transform (FFT). The Discrete Fourier Transform (DFT) transforms a time series (discrete data samples) into an amplitude spectrum (Fourier series components), and the FFT is an efficient computer algorithm for computing the DFT. The DFT of a time series $\{w_i\}$ with m samples is defined by

$$W_n = \sum_{i=0}^{m-1} w_i \exp(-j2\pi ni/m), \quad n=0,1,\ldots,m-1 \qquad (A.5)$$

A straightforward calculation of (A.5) would require m^2 operations (complex multiplication followed by a complex addition). The FFT reduces the number of operations to approximately m times the natural log of m.

APPENDIX II

EQUIVALENT SERIES IMPEDANCE AND SHUNT ADMITTANCE OF TRANSMISSION LINES

In a three-phase transmission line with a total of x bundled conductors and y ground wires, the voltage equation for any harmonic frequency n is given by [21]

$$\begin{bmatrix} \bar{V}_n^1 \\ \bar{V}_n^2 \\ \cdot \\ \bar{V}_n^x \\ 0 \\ \cdot \\ 0 \end{bmatrix} = \begin{bmatrix} \bar{Z}_{11}^n & \bar{Z}_{12}^n & \cdots & \bar{Z}_{1,x+y}^n \\ \bar{Z}_{21}^n & \bar{Z}_{22}^n & \cdots & \bar{Z}_{2,x+y}^n \\ \cdot & \cdot & & \cdot \\ \cdot & \cdot & & \cdot \\ \cdot & \cdot & & \cdot \\ \cdot & \cdot & & \cdot \\ \bar{Z}_{x+y,1}^n & \cdots & & \bar{Z}_{x+y,x+y}^n \end{bmatrix} \begin{bmatrix} \bar{I}_n^1 \\ \bar{I}_n^2 \\ \cdot \\ \bar{I}_n^x \\ \cdot \\ \cdot \\ \bar{I}_n^{x+y} \end{bmatrix} \qquad (A.6)$$

where

$$\bar{Z}_{ii}^n = (R_i^n + R_d^n) + j(2.02233\times10^{-3}) f_o n \ln(D_e^n/D_i) \ \Omega/mi$$

$$\bar{Z}_{ij}^n = R_d^n + j(2.02233\times10^{-3}) f_o n \ln(D_e^n/D_{ij}) \ \Omega/mi$$

$$R_i^n = \frac{R_i^o a_n}{2} \left[\frac{\text{ber } a_n \ \text{bei}' \ a_n - \text{bei } a_n \ \text{ber}' \ a_n}{(\text{ber}' \ a_n)^2 + (\text{bei}' \ a_n)^2} \right] \qquad (A.7)$$

with

$$R_d^n = (1.588\times10^{-3}) f_o n \ \Omega/mi$$

$$D_e^n = (2160\sqrt{\rho \ / f_o})/\sqrt{n} \ \text{ ft}$$

if

$$a_n = (.0636\sqrt{\mu f_o / R_i^o})\sqrt{n} \ .$$

Herein,

ω_o, f_o : Angular and linear fundamental frequencies

R_d^n : Earth resistance at n-th harmonic frequency

D_i : GMR of conductor i

D_{ij} : Distance between conductors i and j

R_i^o : Dc resistance of conductor i

ber,ber': Real Bessel function and its derivative

bei,bei': Imaginary Bessel function and its derivative

ρ : Earth resistivity (=100 Ω for damp earth)

$\bar{Z}_{ij}^n$: Self impedance of conductor i (i=j) and mutual impedance between conductors i and j ($i \neq j$)

Equation (A.6) can be reduced to the partitioned form

$$\begin{bmatrix} [\bar{V}^n] \\ [0] \end{bmatrix} = \begin{bmatrix} [\bar{Z}_1^n] & [\bar{Z}_2^n] \\ [\bar{Z}_3^n] & [\bar{Z}_4^n] \end{bmatrix} \begin{bmatrix} [\bar{I}^n] \\ [\bar{I}^{n'}] \end{bmatrix} \tag{A.8}$$

Eliminating $[\bar{I}^{n'}]$ from (A.8) results in

$$[\bar{V}^n] = [\bar{Z}^n]\ [\bar{I}^n], \qquad [\bar{Z}^n] = [\bar{Z}_1^n] - [\bar{Z}_2^n][\bar{Z}_4^n]^{-1}[\bar{Z}_3^n]. \tag{A.9}$$

For the shunt admittance matrix formulation, the potentials of the line conductors are related to the conductor charges by

$$[\bar{V}^n] = [P][\bar{q}^n] \tag{A.10}$$

where

$$[\bar{V}^n] = [\bar{V}_1^n\ \bar{V}_2^n \ldots \bar{V}^n\ 0\ \ 0 \ldots 0]$$

$$[\bar{q}^n] = [\bar{q}_1^n\ \ \bar{q}_2^n \ldots \bar{q}_{x+y}^n]$$

$$P_{ii} = (1/2\pi\epsilon)\ \ln(H_i/r_i)$$

$$P_{ij} = (1/2\pi\epsilon)\ \ln\ (H_{ij}/D_{ij}),\ \ i \neq j.$$

Herein,

P_{ij} : Potential coefficients ($F^{-1}m$)

$\bar{q}_i^n$: Electric charge of conductor i

ε : Relative permeability

H_i : Distance between conductor i and its image

H_{ij} : Distance between conductor i and image of conductor j

r_i : Radius of conductor i

Similar considerations as for the series impedance lead to

$$[\bar{V}^n] = [C][\bar{q}^n], \quad [C] = [P]^{-1}.$$

Finally, the shunt admittance is found by

$$[Y] = j2\pi f_o n[C]. \tag{A.11}$$

In case of a single-phase transmission line, the series impedance and shunt admittance for the n-th harmonic frequency are respectively given by

$$\bar{Z}^n = R^n + jn\omega_o L^n$$

and

$$\bar{Y}^n = jn\omega_o C$$

where R^n is expressed in (A.7) in terms of its d.c. value and L^n is composed of two components:

$$L^n = L_e + L_i^n$$

L_e is the frequency-independent external inductance given by

$$L_e = \frac{\mu}{2\pi} \ln(D/r).$$

and L_i^n is the internal inductance which is frequency-dependent. L_i^n

is related to its d.c. value by

$$L_i^n = \frac{4L_i^o}{a_n}\left[\frac{\text{ber } a_n \text{ ber' } a_n + \text{bei } a_n \text{ bei' } a_n}{(\text{ber' } a_n)^2 + (\text{bei' } a_n)^2}\right], \qquad \text{(A.12)}$$

VITA

Yahia Baghzouz was born on August 13, 1956, in Beni-Amrane, Algeria. He attended elementary and secondary schools in Algiers, Algeria, graduating from LTGA (Lycee Technique de Garcons d'Alger) high school with honors in May, 1976. In August of 1977, he entered Louisiana State University in Baton Rouge, Louisiana, USA, and received his Bachelor and Master of Science degrees in Electrical Engineering in May 1981 and December 1982, respectively. He has held a research assistantship from June 1981 to July 1985. From August 1985 to the present, he holds an instructor position in the Electrical and Computer Engineering Department. He is a member of Eta Kappa Nu honor society and a student member of IEEE. Presently, he is a candidate for the degree of Doctor of Philosophy in Electrical Engineering.

DOCTORAL EXAMINATION AND DISSERTATION REPORT

Candidate: Yahia Baghzouz

Major Field: Electrical Engineering

Title of Dissertation: Contribution to Power System Harmonic Analysis

Approved:

Major Professor and Chairman

Dean of the Graduate School

EXAMINING COMMITTEE:

Date of Examination:

April 24, 1986